CHAPTER. VI

High Pressure Studies on Ferroelectric Liquid Crystals

6.1 Introduction

The results described in previous chapters deal with studies at atmospheric pressure. Earlier investigations on different liquid crystalline phases have shown that the application of pressure can bring out interesting features.[1,2] However, there have been very few reports[3–'] of either qualitative or quantitative high pressure studies, on ferroelectric liquid crystals (FLC). Since the application of pressure is expected to increase intermolecular interactions' which in turn influence the spontaneous polarization and other ferroelectric properties, it would be of interest to study FLCs under high pressure. This chapter describes the effect of pressure on the spontaneous polarisation (P_s), the rotational viscosity (γ_ϕ), the coercive field (E,) and the transverse dielectric constant $\epsilon_\perp$.

The chapter is organised as follows. First, the high pressure optical set-up that was available in the laboratory[8,9] and the modifications to this set-up made by the author to measure electrical properties are described. Results of P_s, γ_ϕ and E_c

obtained for compounds possessing different magnitudes of P_s are presented. The dielectric constant measured at a few selected frequencies is given. Finally, the $\epsilon_\perp$ data in the smectic A phase has been quantitatively analysed to extract Landau parameters controlling the sof-mode relaxation.

6.2 Experimental

6.2.1 Materials

Three different compounds[10] have been used for these studies. The molecular structure and the phase transition temperatures for the three compounds are given in table 6.1, along with their respective P_s values at $T_c - 10^oC$. Whereas C_7 and A_{11} show isotropic to sniectic A transition, D_8 has a cliolesteric phase above the A phase.

6.2.2 High pressure set-up

The design of high pressure set-up for the study of liquid crystals poses certain problems not normally encountered in the study of solids, for example the containment of tlie sample, the chemical reactivity with tlie material of the container, a proper pressure transmitting medium, etc. The existing high pressure set-up in tlie laboratory had been fabricated by taking all these points into consideration. The set-up has been used only to map phase diagrams in the pressure temperature plane by employing the optical laser transmission method. The author has made some modifications to the set-up such that it can in addition be used to measure some electrical properties like dielectric constant, spontaneous polarisation, etc. In the following a brief description of the existing optical high pressure set-up is given followed by the details of tlie modifications done to measure the electrical properties.

A schematic diagram of tlie high pressure optical set,-up is shown in figure 6.1.

Table 6.1

Compounds used and their P_s values

D8

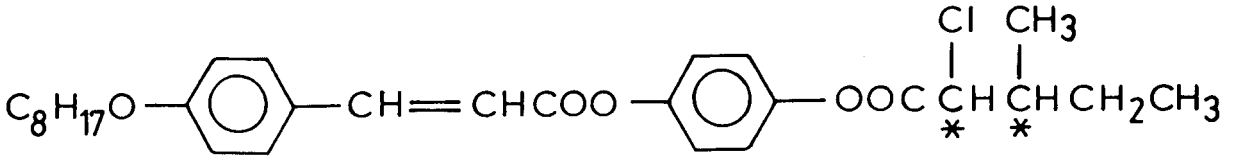

P_S at $T_C - 10^\circ C$ = 1400 $\mu C / m^2$

C_7

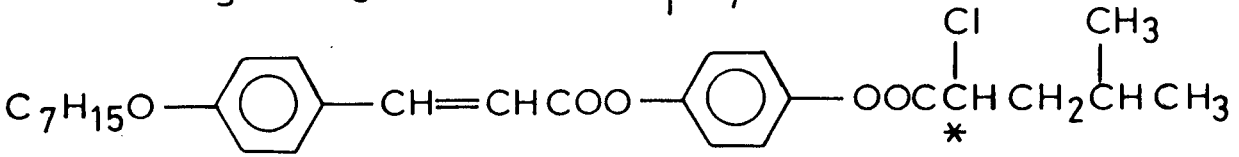

P_S at $T_C - 10^\circ C$ = 960 $\mu C/m^2$

A_{11}

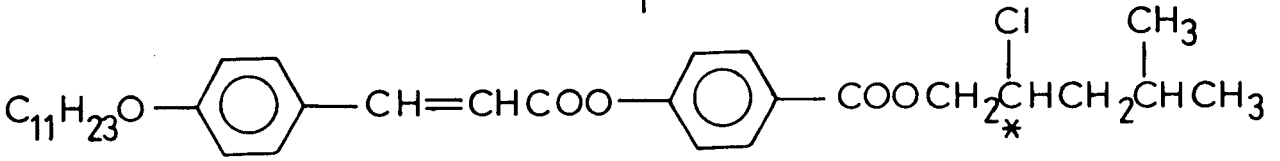

P_S at $T_C - 10^\circ C$ = 395 $\mu C/m^2$

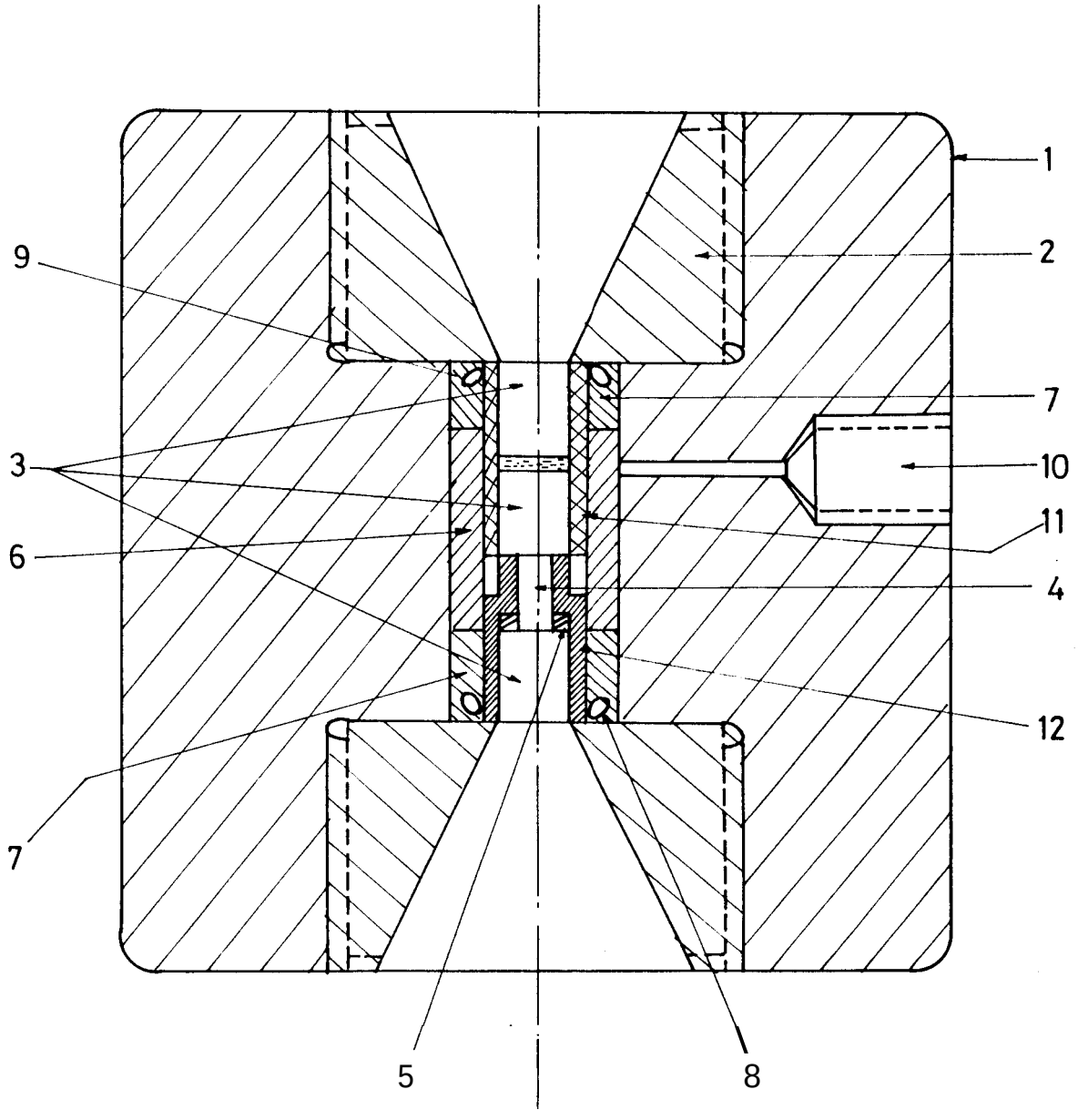

1. CELL BODY 2. STEEL PLUG 3. SAPPHIRE CYLINDERS
4. GLASS ROD 5. WASHER AND SPRING 6. CENTRE SPACER
7. OUTER SPACER 8. 'O' RING 9. ANTIEXTRUSION RING
10. HIGH PRESSURE CONNECTION 11. FLURAN TUBE 12. LOW-PRESSURE SEALER

FIG. 6.4. HIGH PRESSURE OPTICAL CELL

Most of the components of tlie cell are made using a low alloy hardened steel (EN24). The body of the cell has threaded openings on both sides into which two plugs with exactly matching threads are fitted. On the outside, the plugs have a large tapered opening (SO^o outside taper) which facilitates a wide viewing angle without affecting the strength of tlie plug. On the inside, the plugs have small optically flat protrusions. These plugs keep the sample assembly in position. The central hole of tlie upper plug is sealed by an optically polished sapphire rod which is a part of the sample assembly. To avoid any possible leakage of the oil through the clearance between the plug and the sample assembly, a neoprene 'O' ring and an anti-extrusion ring are placed around the junction. A small washer made of aluminium foil fills any crevices on the surface of the plug and completely seals the assembly. The proper positioning of tlie sample assembly is ensured by the use of centre and outer spacers.

6.2.3 The sample assembly

The sample assembly is schematically shown in figure 6.2. The sample is sandwiched between two sapphire rods which fit snugly inside a fluran tube. Fluran is an elastonier having excellent desirable properties: (i) it transmits pressure exceedingly well and withstands temperatures up to 270°C, (ii) it does riot react with the liquid crystalline material. Wrappirig a thin steel wire around the fluran tubing on tlie sapphire windows ensures a complete isolation of tlie sample from the pressure transmitting medium.

The sample assembly along with a low pressure sealer and a glass rod are placed inside two outer spacers and tlie centre spacer (see Fig.G.l). The upper sapphire seals the top end and the bottom end is sealed by a third sapphire which does not form a part of the sample assembly.

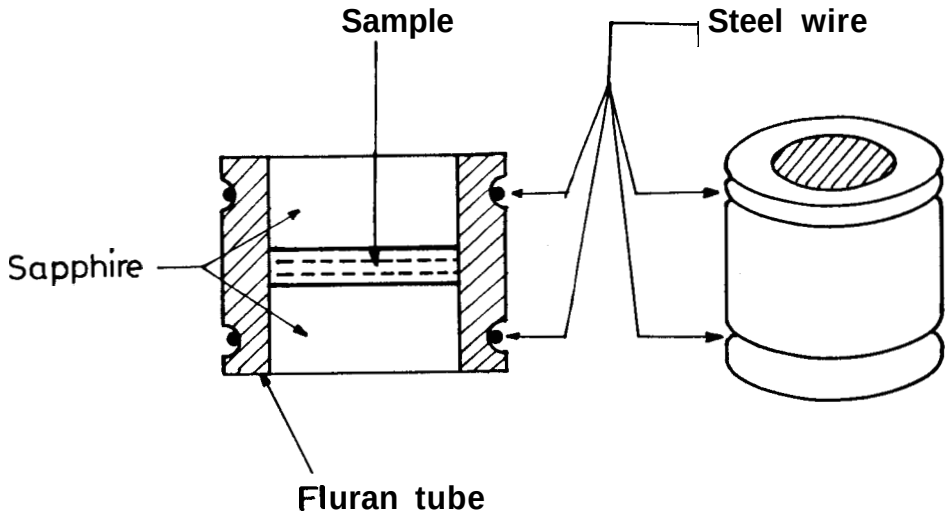

Fig.6.2. Sample assembly.

6.2.4 Temperature control and measurement

The pressure cell was push fitted inside an aluminium cylinder. Nichrome tape wound on mica sheets and wrapped around the inside wall of the aluminium cylinder scrvcs as an electrical heater with an effective heating capacity of about 200 watts. A chromel-alumel thermocouple sheathed in a ceramic tube was used to measure the temperature sensed by tlie sample. The thermocouple was calibrated using several substances exhibiting sharp phase transitions. The accuracy in the measurement of temperature is reckoned to be $\pm$ 10 mK.

6.2.5 High pressure plumbing system

A schematic diagram of the high pressure plumbing system is shown in figure **6.3.** A hand pump (PPI, USA) is used as a pressure primer. The required pressure is fine tuned with the help of a pressure generator (HIP, USA) having a small displacement capacity. The line pressure which is the same as the pressure experienced by the sample, is measured by a Bourdon type (Heise) gauge.

6.2.6 Determination of phase transition temperatures

Light from a He-Ne laser (Spectra Physics Model) was made to fall on the sample in the optical cell and the transmitted intensity was detected using a photo transistor (MRD 300). The voltage drop across a $1k\Omega$ resistor caused by the photo current was measured using a digital voltmeter. A parallel connection from this was taken to one of the channels of a multichannel recorder (Linseis, Model 2041) through a low voltage DC source. Using the voltage source as an off-set control, small intensity changes over and above a large background intensity could be easily monitored. The temperature of the sample was measured by measuring the output of the thermo-

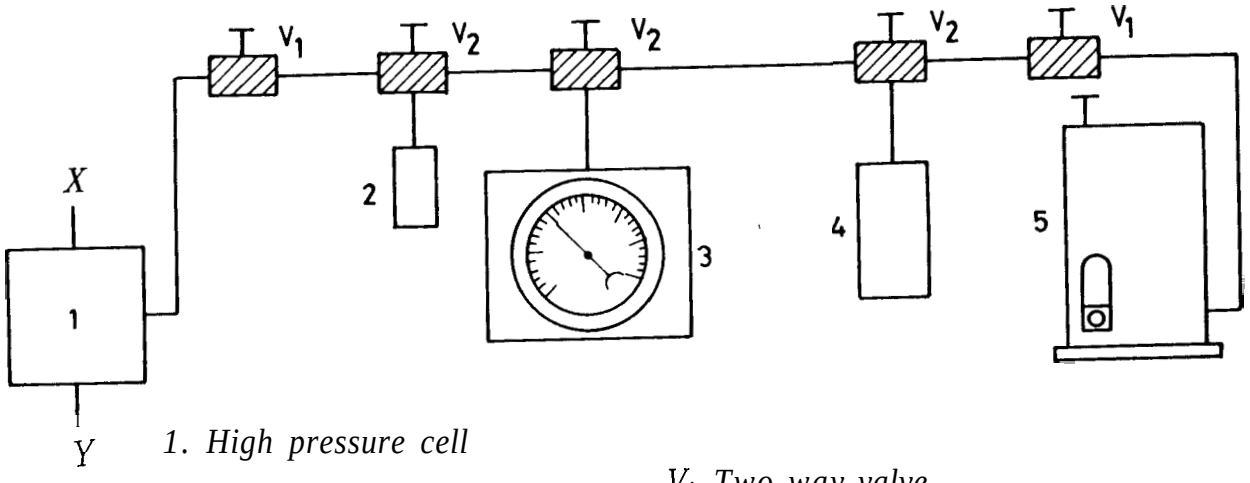

1. High pressure cell

2. Pressure transducer

3. Bourdon gauge

4. Pressure generator

5. Hand pump

V_1 *Two-way valve*

V_2 *Three-way valve*

X,Y: Electrical leads

Fig.6.3. High pressure plumbing system.

couple in conjunction with a low drift digital nanovoltmeter (Keithley 181). The voltage output of the thermocouple was fed to another channel of the multichannel recorder. Thus both the intensity and temperature could he simultaneously monitored and recorded. Abrupt changes in intensity of the transmitted light occurring at the phase changes was used to determine the transition temperatures.

6.2.7 Electrical set-up

The existing high pressure optical set-up was modified to measure electrical properties. While making modifications the following points were kept in mind.

1. The same basic set-up should he usable for both optical and electric set-up.
2. The sample container should enable application of electrical field
3. The sample assembly must be completely electrically isolated from the rest of the high pressure equipment.

Modifications

1. Tlie two sapphire rods serving as sample containers and the third sapphire used for seating the window were replaced by optically polished steel rods (cylinders) of exactly the same dimension. The steel cylinders also perform the job of electrodes. Screws threaded into the cylinders established contact between the sample and the measuring equipment.
2. Electrical isolation of the sample assembly was ensured by using mylar washers instead of aluminium washers for the window sealing and by using a teflon sleeve on the low pressure sealer.

As in the optical set-up the sample thickness was defined by a teflon spacer (thickness 60 $\sim$ μm). The surfaces of the steel cylinders coming in contact with the sample were coated with polyimide solution and rubbed unidirectionally to get planar orientation of the molecules.[11]

The data presented here were obtained from three independent measurements, a fresh sample being loaded in the high pressure cell each time. The good reproducibility of tlie data showed that tlie alignment of tlie sample was very good.

Measurement of spontaneous polarisation P_s

The calibrated Diamant bridge[12] set-up described in chapter I1 was employed to measure tlie P_s. The advantage of this method, as already noted, is that tlie hysteresis loops give additional information regarding the coercive field E_c and the rotational viscosity γ_ϕ.[13] However, as will be seen later, tlie field required to unwind tlie helix increases at high pressures and as such tlie probing field has to be high. For this purpose, the output of the function generator was amplified using a high voltage amplifier (Kepco, BOP 1000M). Because of the restricted dimension of the electrode (steel cylinder) tlie active area of tlie sample is quite small ($\sim 0.15 cm^2$) and consequently tlie amplitude of the signal from the sample would also be small. This was overcome by amplifying the sample signal using a programmable gain difference amplifier (AD 524). The data collection and analysis were handled by a microcomputer in conjunction with a high speed data acquisition system (HP 7090A), the details of which have already been described in chapter II. Since it is not possible to determine the active area of the sample 'in-situ', we proceeded as follows. The P_s data as obtained in the high pressure cell at 1 bar was compared with the P_s values determined using a ITO coated glass cell at room pressure and a conversion factor was obtained. It is important to note that the P_s values obtained on the increasing

and decreasing pressure cycles were in excellent agreement with each other proving thereby tliat tlie sample dirnensions did not change on pressure cycling. From the hysteresis loops, rotational viscosity γ_ϕ was extracted as explained in chapter IV. These loops also provide tlie value of the coercive field E_c which corresponds to the value of tlie applied voltage at the instant $P_s = 0$ and which gives a measure of the critical unwinding field.

Dielectric measurements

The dielectric constant was measured hy making capacitance measurements using a versatile variable frequency Impedance analyser (HP 4192A). The data acquisition and the temperature control were handled by a microcomputer. The details are already given in Chapter III. In this set-tip, since the spacer material is present in the electrically active area, the measured capacitance would include its contribution also. In order to overcome these problems we followed the following procedure. The sample in the high pressure cell was maintained at atmospheric pressure. The capacitance values obtained far away from the $A - C^*$ transition in both the A and C^* phases were compared with the tlielectric constant values got from a measurement done at room pressure using a regular ITO coated glass cell. This yielded a conversion factor to calculate $\epsilon_\perp$ values from capacitance measurements. The values obtained on both increasing arid decreasing pressure cycles were in excellent agreement with each other proving thereby that the sample dimensions (area and thickness) did not change on pressure cycling and in addition that there is very little "pressure hysteresis".

Both P_s and dielectric constant measurements were always conducted along isobars, i.e, tlie measurements were made by keeping tlie pressure constant and varying the temperature at a uniform sate of 6°C/hour away from the transition and

at 2^{o}C/hour close to the transition.

6.3 Results and Discussion

6.3.1 Pressure-Temperature (P-T) phase diagrams

Figures 6.4-6.6 show tlie P-T diagrams for the three cornpounds C_7, A_{11} and D_8 respectively. A common feature observed is that tlie temperature range of the smectic A phase, a factor which is known to influence the nature of the $A - C^*$ transition,[14,15] increases with pressure, although the extent of increase is different for different compounds (4.8^{o}/kbar, 1.7^{o}/kbar, 5.3^{o}/kbar respectively). This behaviour is in agreement with earlier reports[3,4] on phase diagrams of ferroelectric compounds at high pressure. It is also seen from the figures that in all the three compounds the phase boundaries are linear. We have fitted the optical transmission data to an equation of the form $T_c(P) = A_1P + A_2$. The values of the constants A_1 & A_2 for tlie three compounds are given in table **6.2.** The open circles in the figures represent the T_c values obtained frorn P_s measurements the solid line is the fit to the optical data. It is clear from the figures that there is an excellent agreement between T_c values obtained by optical transmission method and P_s measurements. This also confirms the purity of tlie compound in the high pressure cell environment.

6.3.2 P_s measurements

Figure 6.7 is a plot of D-E hysteresis loops obtained using the Diamant bridge method for C_7 at 1 bar (room pressure), 1 khar and **2** khar. The salient features, with increasing pressure, observed are:

1. The electrical displacement D and hence P_s decreases

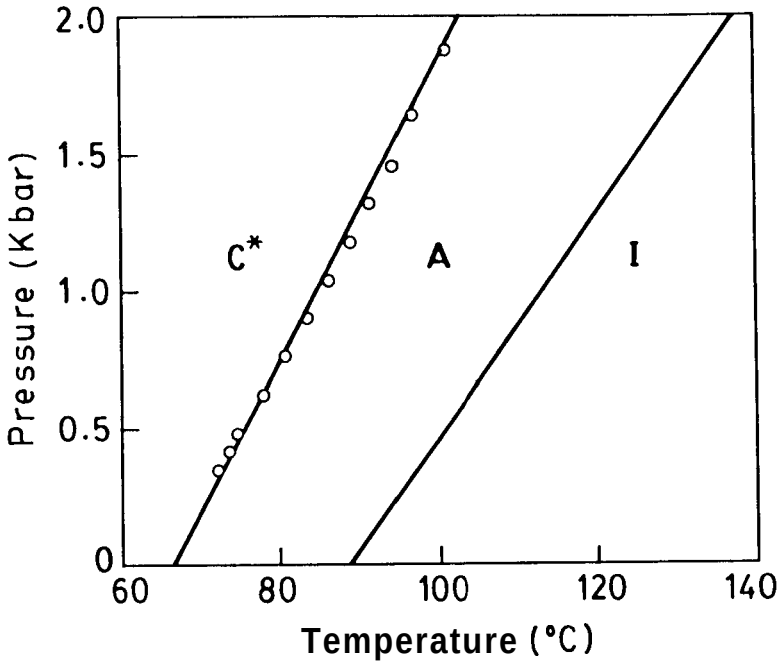

Fig.6.4. P-T diagram for C7. Solid lines are the fits to the optical transmission data and the circles, the values from P_s measurements.

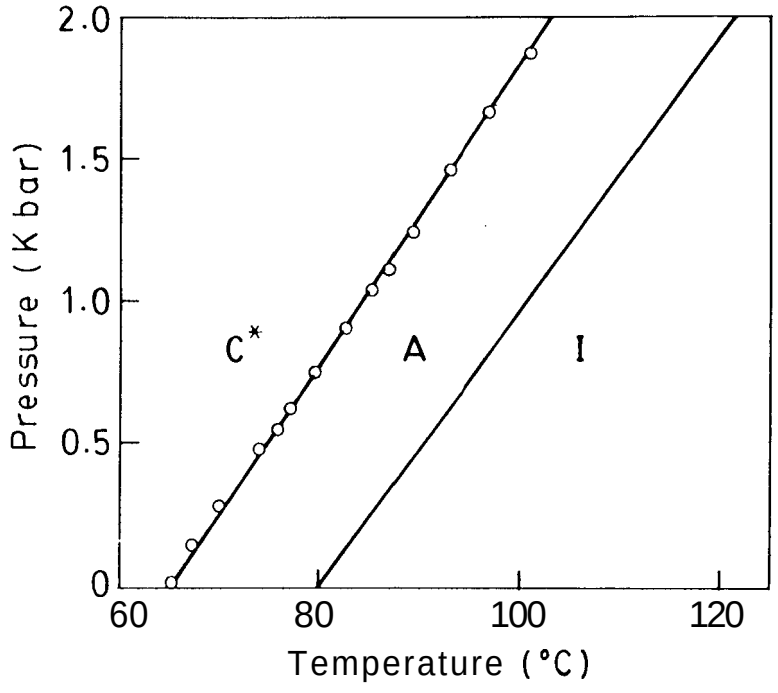

Fig.6.5. P-T diagram for A_{11}. (see legend of Fig. 6.4).

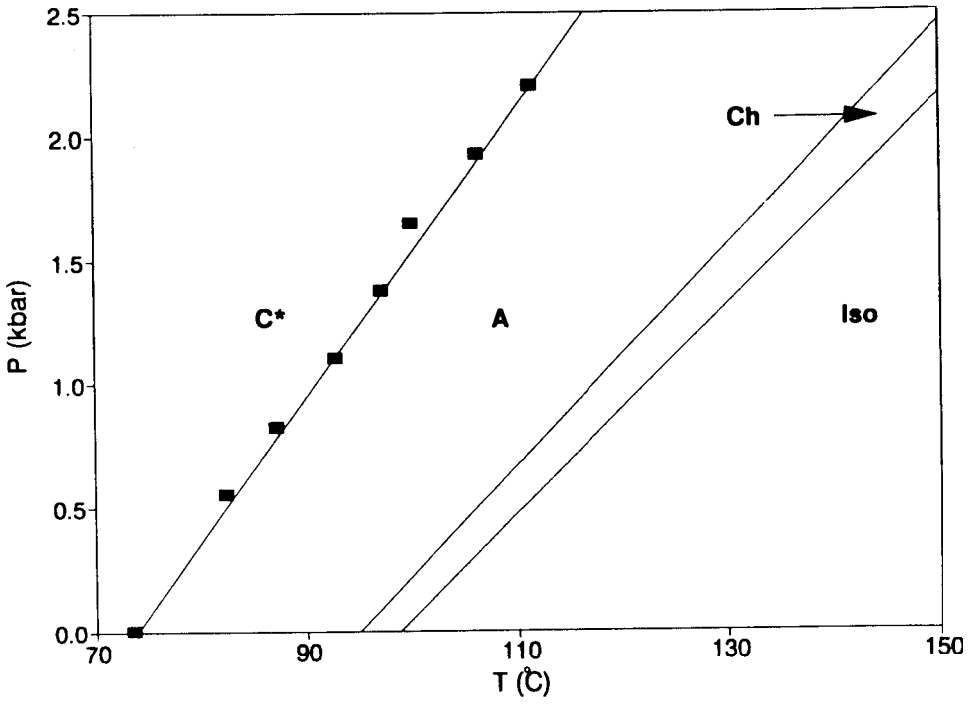

Fig.6.6. P-T diagram for D8. (see legend of Fig.6.4).

Table 6.2

Values of constants A_1 & A_2 obtained by fitting the optical transmission data to an equation $A_1 P + A_2$

Compound	A_1 °C/kbar	A_2 °C
A_{11}	18.8	65.2
C_7	17.9	66.5
D_8	17.1	**73.93**

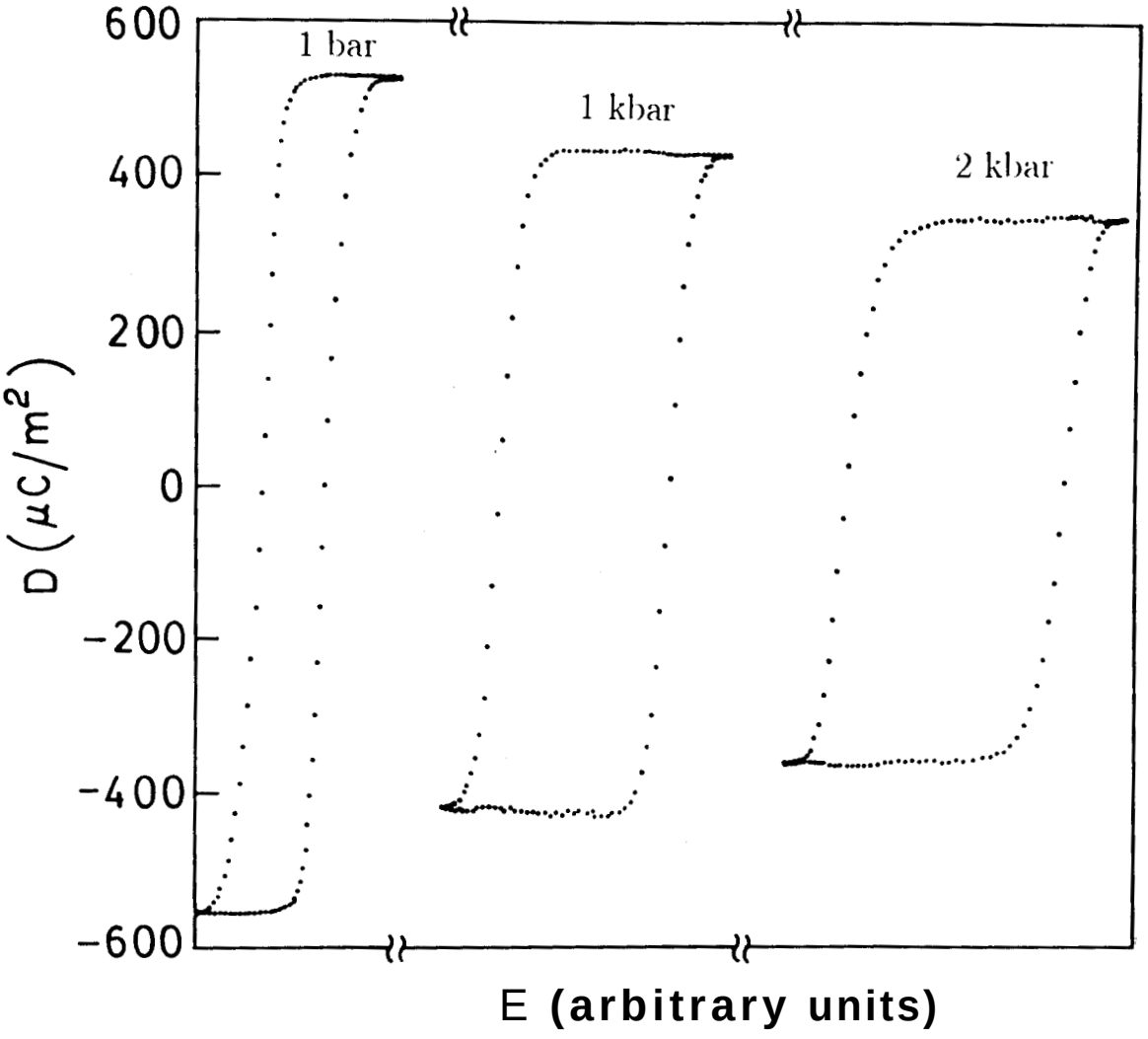

Fig.6.7. Hysteresis loops obtained for C7 at (a) 1 bar, (b) 1 kbar and *(c)* 2 kbar.

2. 'The coercive field E_c increases considerably.

Figures 6.8 and 6.9 are plots of the temperature variatioris of P_s at different pressures for the compounds C_7 and D_8 respectively. It is seen that at a given relative temperature T_c – T, the magnitude of P_s decreases substantially witli increasing pressure. This variation of P_s with pressure is shown in figures 6.10 to 6.12 for the compounds D_8,C_7 and A_{11} respectively. The $\frac{dP_s}{dP}$ values, obtained by fitting the data to a straight line, are 20 μC/kbar, 30 μC/kbar and 10 μC/kbar for the three compounds. In contrast to this if the temperature is kept constant then P_s value increases with pressure as seen from figure 6.13 for the conipound D_8.

Another notable feature seen in figures 6.8 and 6.9 is that the rate of change of P_s with temperature $\frac{dP_s}{dT}$, evaluated close to the transition, decreases with increasing pressure. To quantify this we have fitted P_s data, for the cornpound C_7 at each pressures to a simple power law of the type $P_s = P_o(T_c - T)^{\beta}$. The value of β for C_7 at room pressure is 0.44 and at 2 kbar it is 0.68. That is the value of β shows a marked increase with increasing pressure . This observation is different from the earlier observations[5] on the compound DOBAMBC which has a low value of P_s. For DOBAMBC they got $\beta = 0.48$ at 1 bar and 0.38 at 2 kbar.

The decrease in P_s with increasing pressure is rather strange because application of pressure is known to increase the intermolecular interactions resulting in an increase in the rotational viscosity γ_ϕ which in turn enhances the biasing effect of the free rotations of the molecule. Thus P_s should have increased with pressure. One possible reason for the observed behaviour may be that the tilt angle may be decreasing with increasing pressure. However we do not have a direct proof of this.

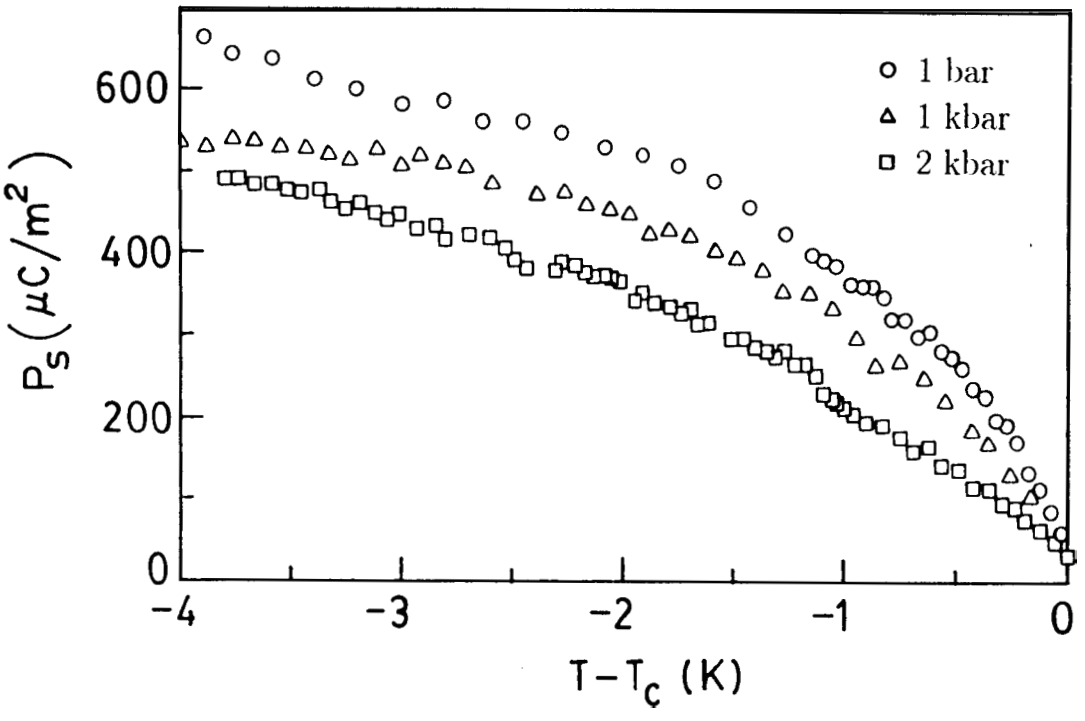

Fig.6.8. Thermal variation of P_s obtained for C7 at (a) 1 bar, (b) 1 kbar and *(c)* 2 kbar.

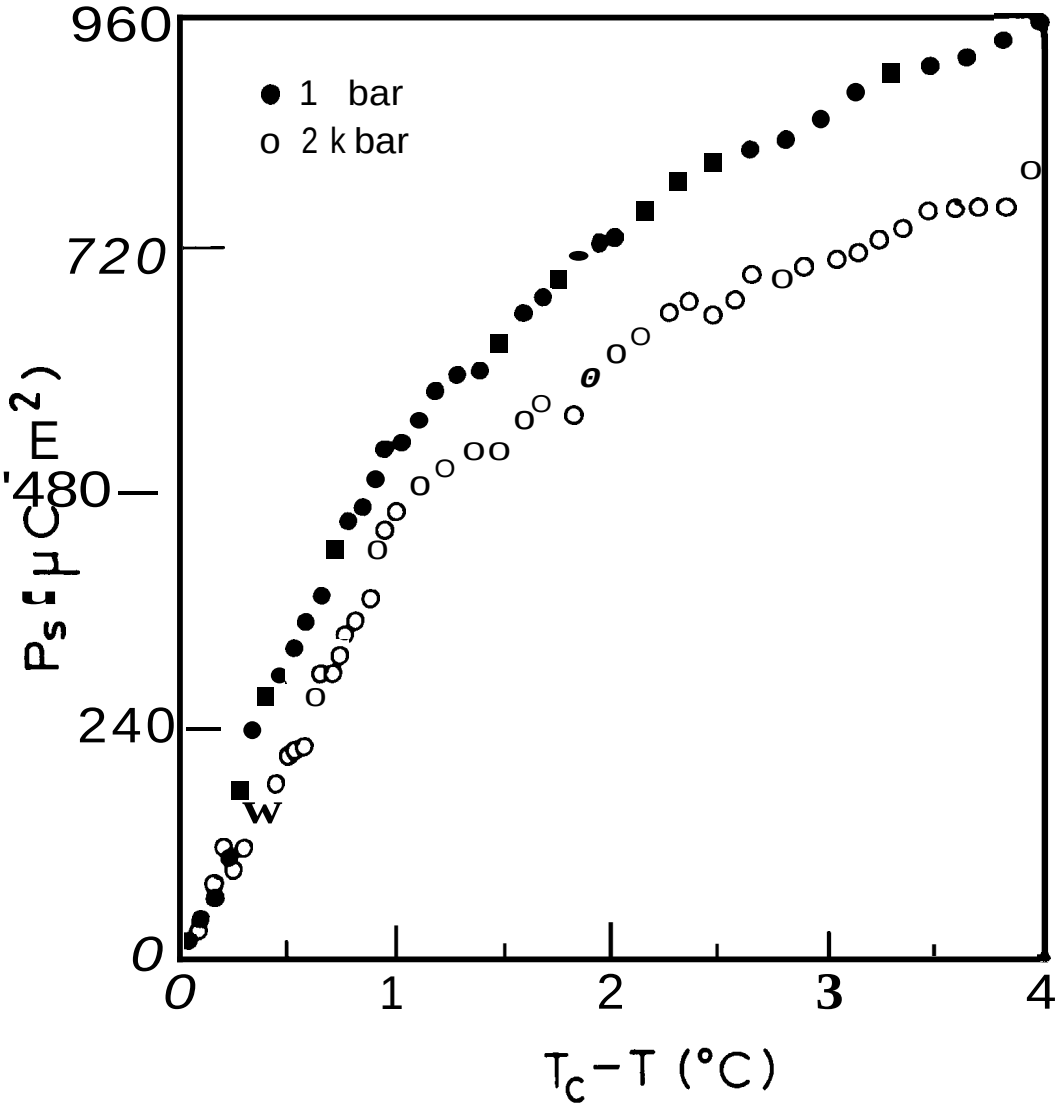

Fig.6.9. Thermal variation of P_s obtained for D8 at (a) 1 bar and (b) 2 kbar.

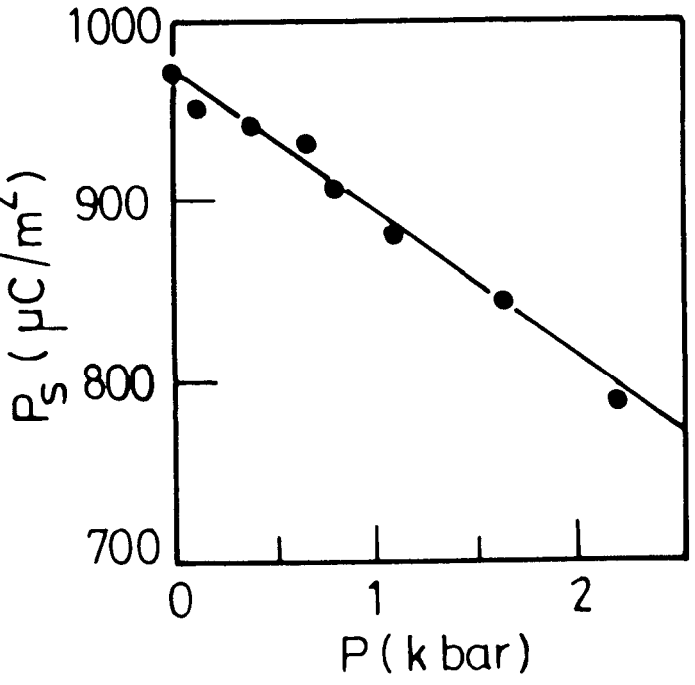

Fig.6.10. Effect of pressure on P_s for DS; (●) experimental data, (—) fit to a straight line.

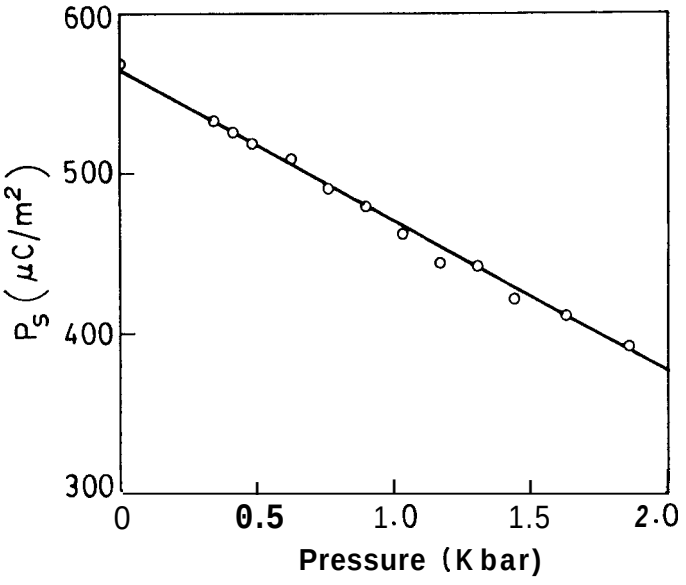

Fig.6.11. Effect, of pressure on P_s for C7; (○) experimental data, (—) fit to a straight line.

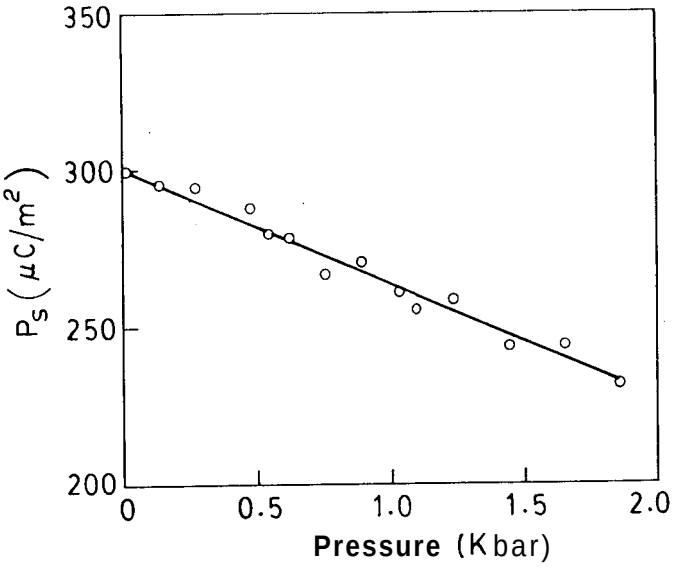

Fig.6.12. Effect of pressure on P_s for A_{11}; (○) experimental data, (—) fit to a straight line.

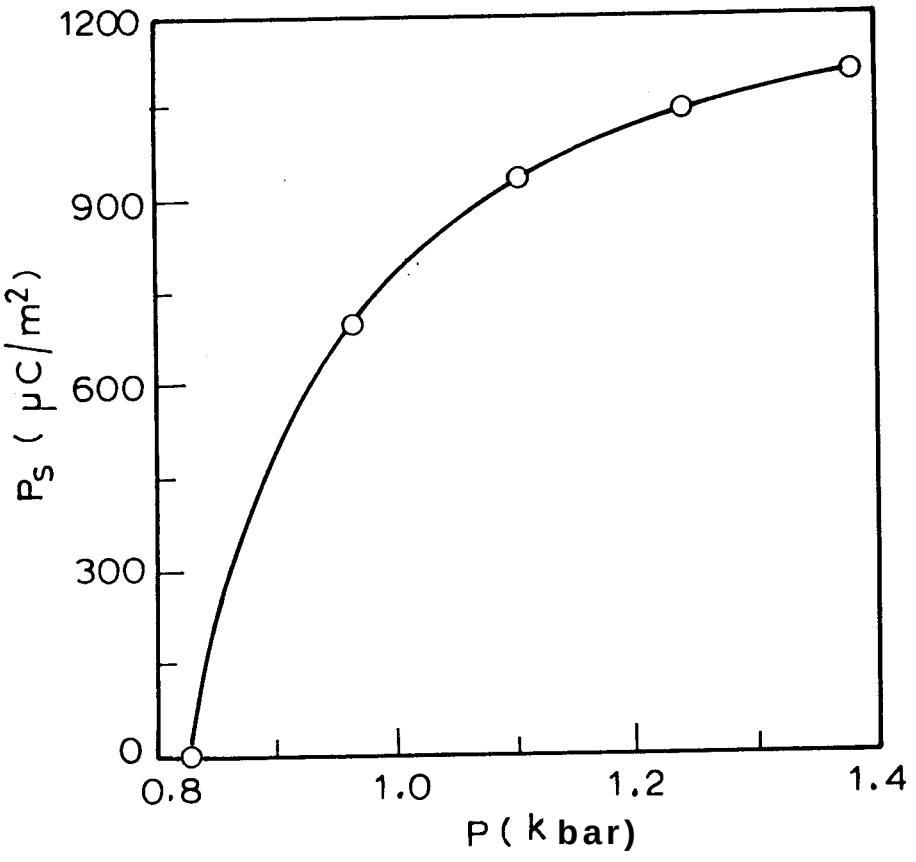

Fig.6.13. Influence of pressure on the magnitude of P_s at constant temperature (T = 87.7°C).

6.3.3 Rotational viscosity γ_ϕ

Figures 6.14 and 6.15 are tlie semilogarithmic plots of γ_ϕ at different pressures for the compounds C_7 arid D_8 respectively. It is seen from tlie figures that γ_ϕ increases with increasing pressure. For both the compounds the behaviour is Arrhenius away from the transition, but deviates from it close to the transition. This is true at room pressure as well at high pressure. The pressure variation of γ_ϕ at a constant relative temperature from T_c is shown in figures 6.16 and 6.17 for C_7 and D_8 respectively. For both the compounds the variation is linear with a slope of 0.036 Pa.S and 0.081Pa.S for C_7 and D_8 respectively. One cause for the increase in γ_ϕ with pressure is, as mentioned earlier, the increase in molecular interactions with pressure. An important consequence of the increase in γ_ϕ with pressure will be discussed in next section.

6.3.4 Coercive field E_c

As seen qualitatively from figure 6.7, the coercive field increases substantially with increase in pressure. Figure 6.18 is a plot of E_c vs. reduced temperature (T_c – T) at 1 bar and 2 kbar for D_8. The pressure variation of E_c at a constant relative temperature of T_c – 2°C is shown in figure 6.19. The variation can be described by a straight line with a slope of 1.96kV/cm. Thus from the ahove studies it is clear that the increase in pressure reduces P_s and increases both γ_ϕ and E_c.

It is well known that the coupling between P_s and the primary order parameter θ is not purely linear and biquadratic coupling terms play a significant role. If the coupling is purely linear the value of the exponent β should riot exceed tlie mean field value of 0.5.[16] But as we saw earlier for C_7, β increases to a value of about 0.68 at high pressure. β being higher than 0.5, indicates that there is an appreciable influence

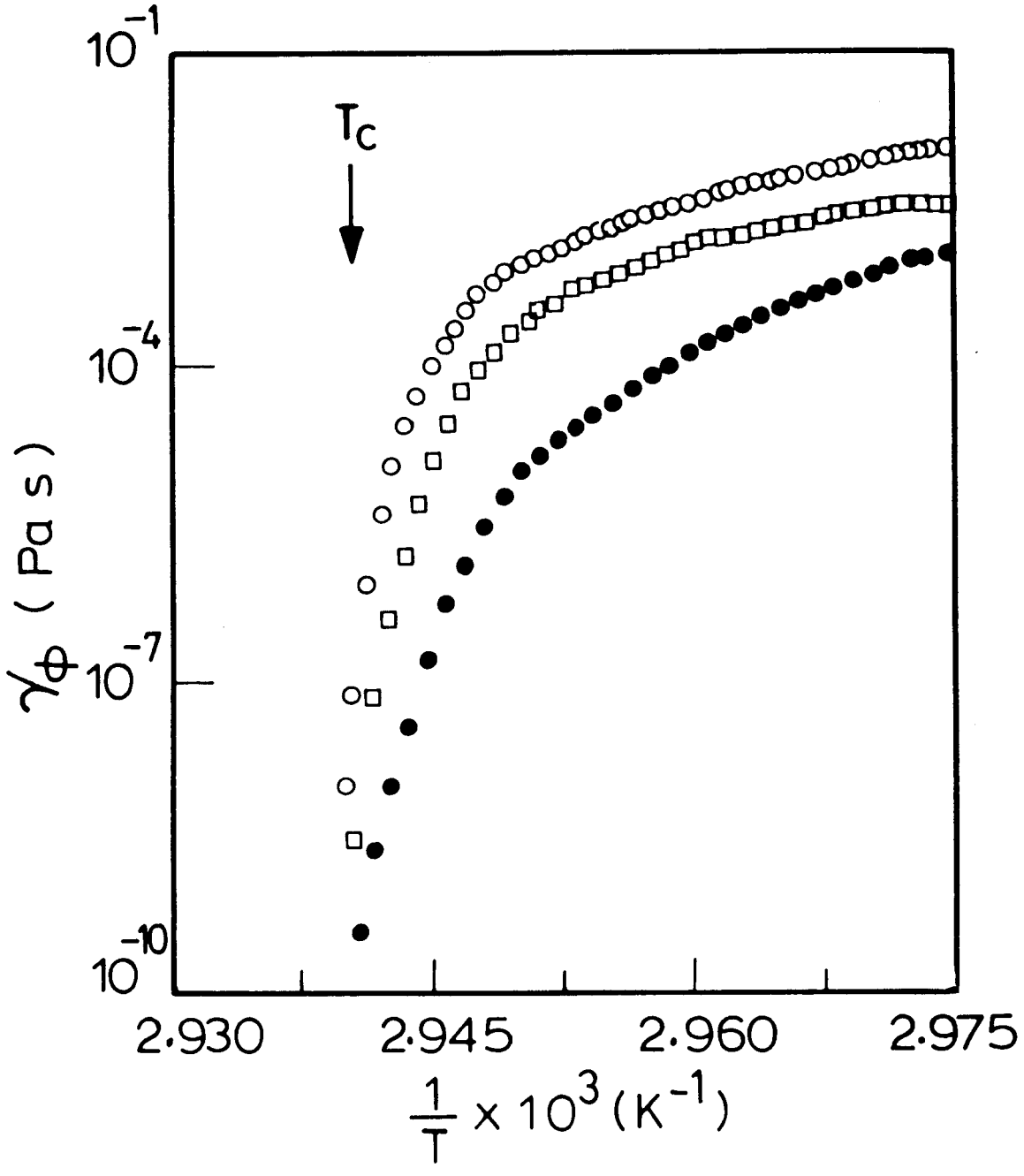

Fig.6.14. Plot of γ_ϕ vs. 1/T for C7 at 1 bar (•), 1.0 (⊖) and 1.9 kbar (○).

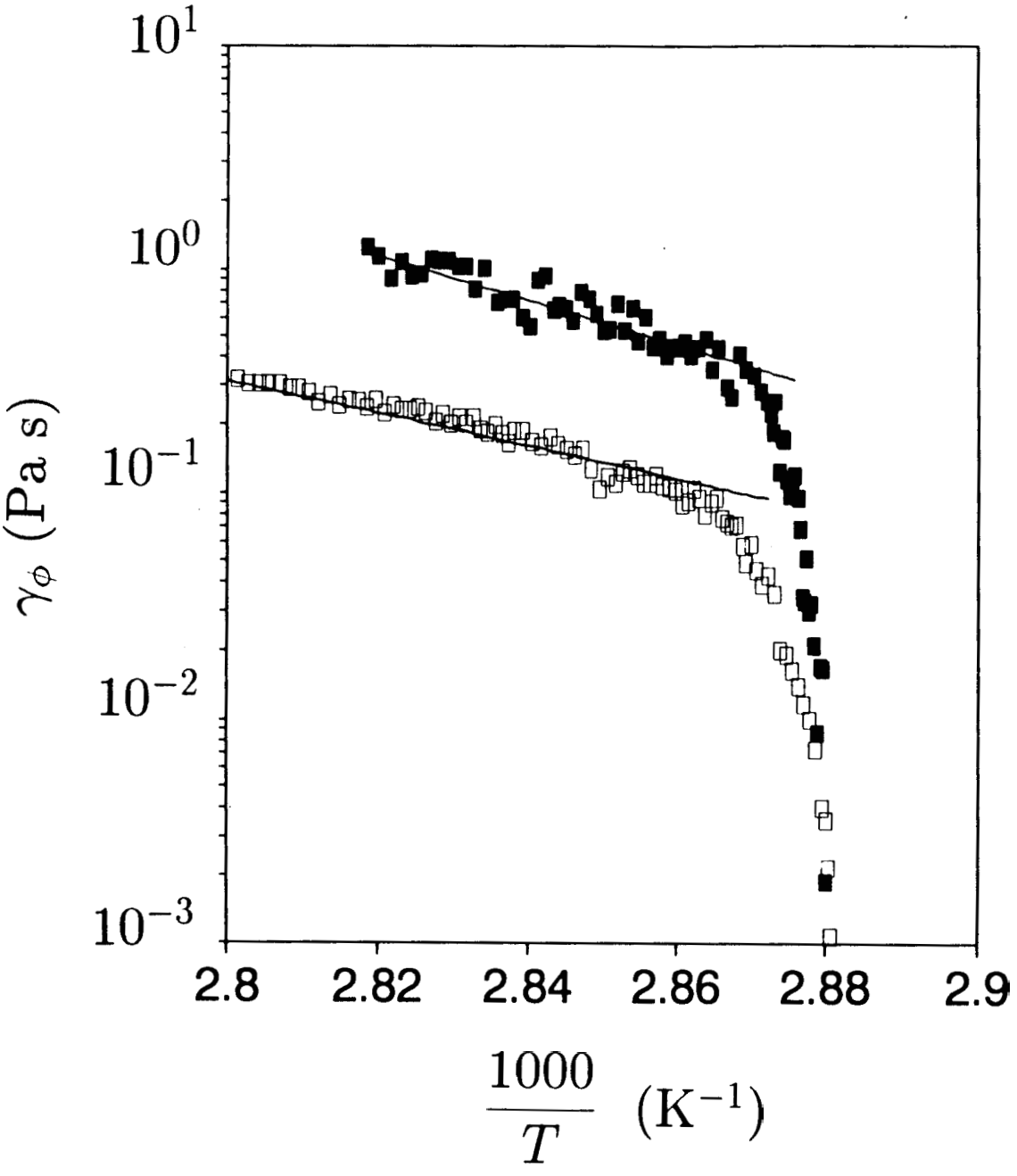

Fig.6.15. Plot of γ_ϕ vs. 1/T for D8 at **(a)** 1 bar (□), (b) 2 kbar (■).

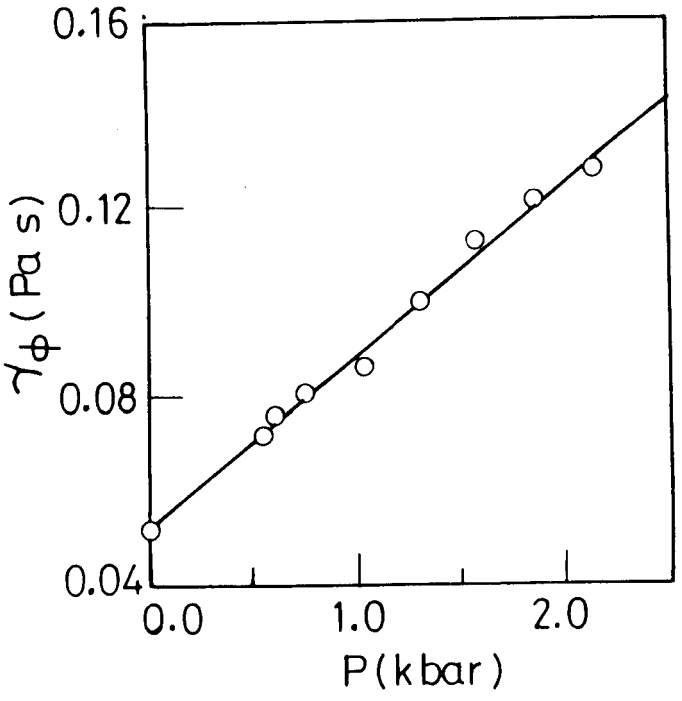

Fig.6.16. Dependence of γ_ϕ on pressure for C7 at $T_c - 4°C$ (○) experimental data, (—) fit to a straight line.

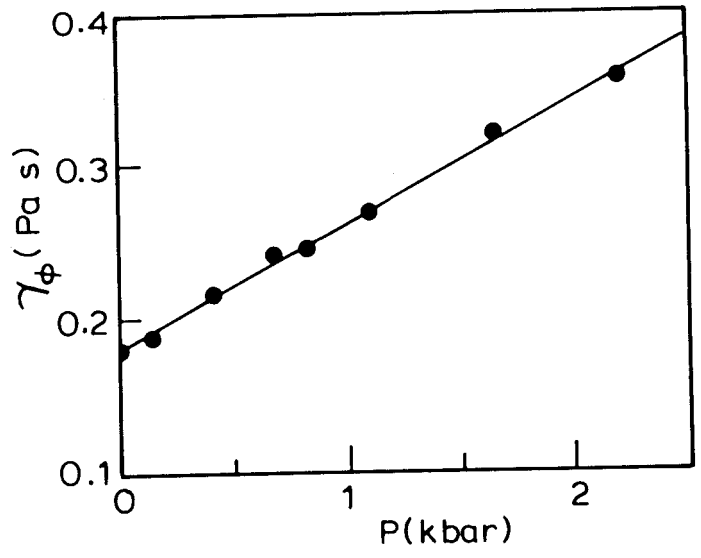

Fig.6.17. Dependence of γ_ϕ on pressure for D8 at $T_c - 4°C$ (●) experimental data, (—) fit to a straight line.

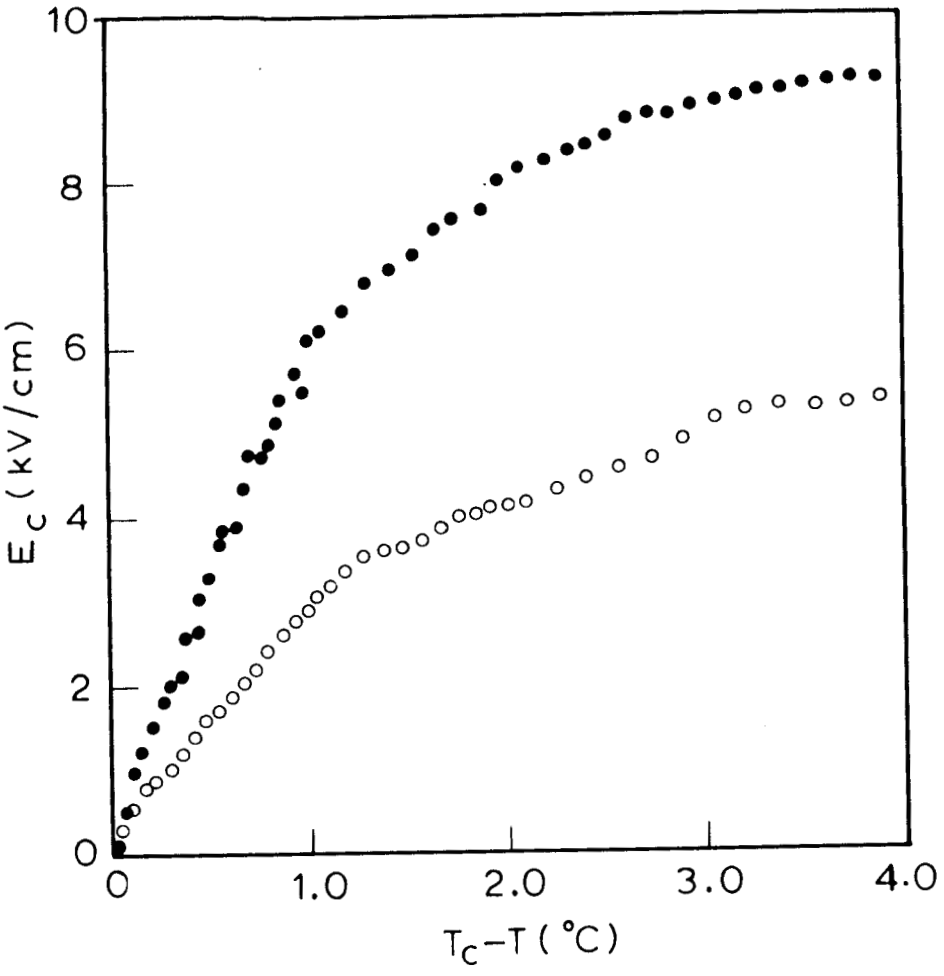

Fig.6.18. Thermal variation of E_c obtained for D8 at (a) 1 bar (○) and (b) 2 kbar (●).

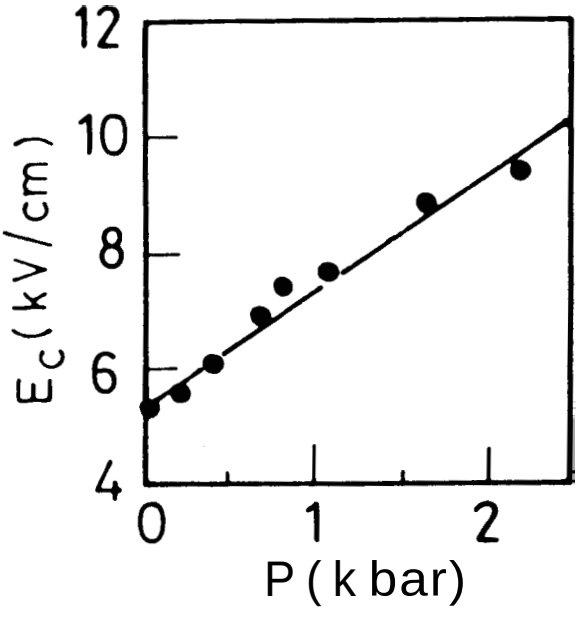

Fig.6.19. Influence of pressure on E_c, (●) experimental point, (-) fit to a straight line.

of lion-linear coupling terms. Indeed it appears that the relative contribution of tlie linear term decreases with increasing pressure. This is a surprising result since the coefficients of the coupling terms are generally assumed to be tlie cliaracteristic of tlie material. Another factor which could have brought about a change in β is tlie mean field to tricritical point cross-over phenomena observed generally in compounds exhibiting $A - C^*$ transitions.[17] All the experiments conducted at room pressure indicate tliat the nature of such a cross-over is governed by the temperature range of the sniectic A phase[15] and/or tlie strength of the transverse dipole moment of the constituent molecule.[18] As seen from figures 6.4-6.6 tlie range of A-pliase does increase with pressure. In order to see whether the transverse dipole moment of the molecule plays a significant role in defining the value of β, we have measured the transverse dielectric constant $\epsilon_\perp$ across the $A - C^*$ transition as a function of pressure. The results are described below.

6.3.5 Static dielectric constant

Even though the structure and hence the true dipole moment of the molecule remain invariant, the effective dipole moment may vary with pressure. To a first approximation, the static transverse dielectric constant can he taken as a measure of the effective dipole moment. Since the P_s data appears to indicate a possible decrease in tlie effective dipole moment, to verify this, we have studied the pressure dependence of $\epsilon_\perp$ of a FLC. Figure 6.20 is a plot of temperature variation of $\epsilon_\perp$ at different pressures for tlie compound D_8. It is seen that in tlie C* phase $\epsilon_\perp$ decreases drastically with pressure whereas in A phase the variation is not much. Similar features were observed by Yesuda *et al.*[5] in DOBAMBC. One factor that could contribute to this behaviour is that the Goldstone mode relaxation frequency f_G may be decreasing with increasing pressure and consequently the response of the system at the mea-

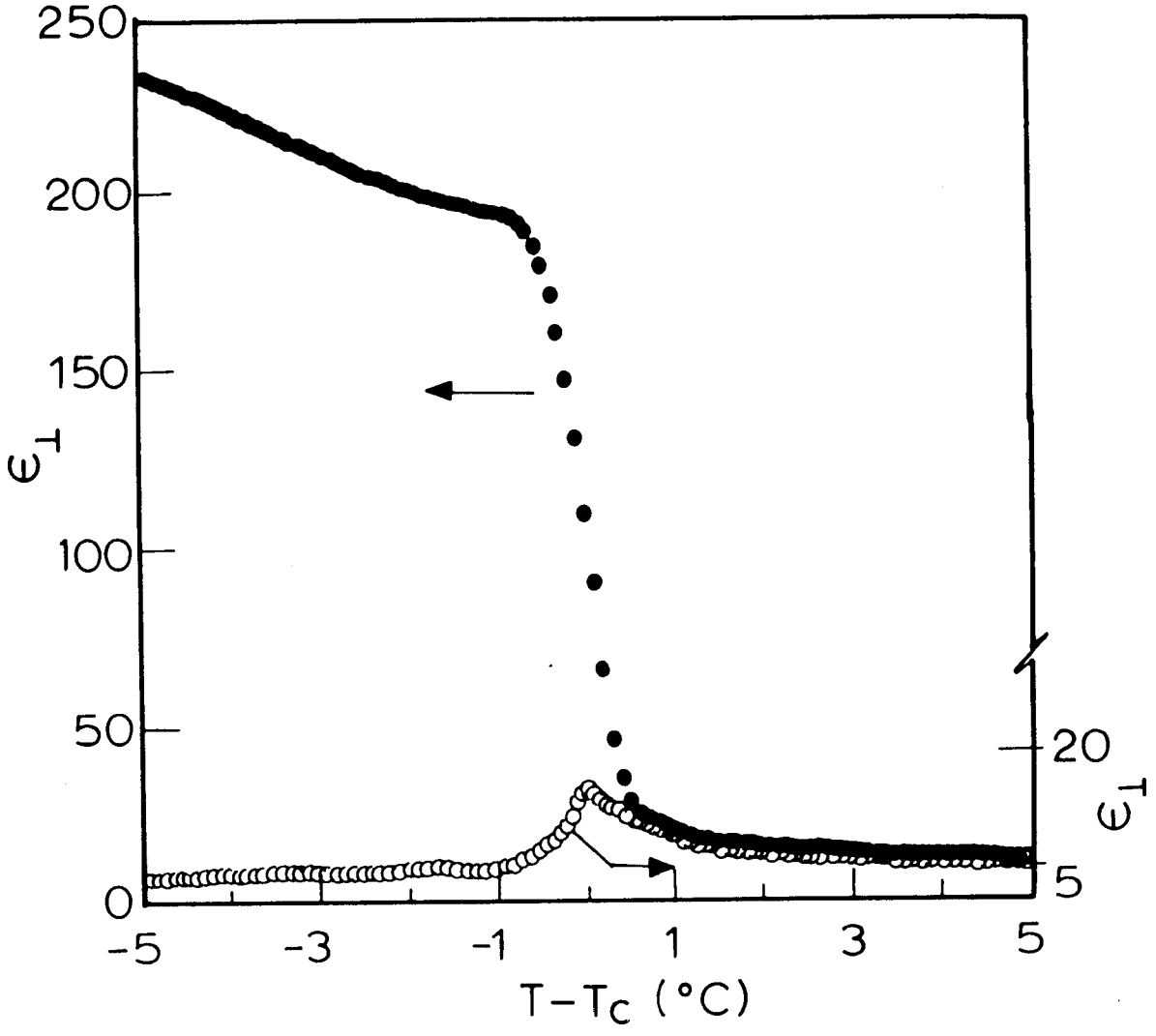

Fig.6.20. Variation of $\epsilon_\perp$ with temperature, (●) at 1 bar and (○) 2 kbar.

suring frequency can not be considered as static. The fact that γ_ϕ increases with pressure supports this view.

6.3.6 Frequency and Pressure dependence of dielectric constant

The above results show that pressure influences the Goldstone mode relaxation strongly. In order to study the effect of pressure on GM and SM explicitly we have measured the dielectric constant $\epsilon_\perp$ for the compound D_8 as a function of pressure at different frequencies. These results are described below.

Figures 6.21a and 6.21b are the surface plots of $\epsilon_\perp$ as a function of frequency (f)and temperature (T)obtained at room pressure. Note the clear existence of two relaxations: the low frequency GM with large amplitude (Fig. 6.21a) and the high frequency SM with a smaller amplitude (Fig. 6.21b). Keeping this information in mind we now examine the effect of pressure.

Figure 6.22a is the plot of $\epsilon_\perp$ as a function of pressure when both T (=92°C) and f (=50 Hz) are kept constant. It is seen that at low pressures, $\epsilon_\perp$ is weakly dependent on pressure but on approaching the $A - C^*$ transition pressure P_c (P_c is the A-C* transition pressure at T = 92°C) it increases rapidly. This behaviour is similar to the thermal variation of $\epsilon_\perp$ at constant pressure (1.1 kbar) and frequency (50 Hz), figure 6.22b, on cooling the sample from the A to the C* phase. Figure 6.23 shows a plot of $\epsilon_\perp$ as a function of pressure at a given relative temperature (T_c - 4)°C for the compound D_8. $\epsilon_\perp$ is observed to decrease drastically with increasing pressure.

Figure 6.24 shows a perspective view of the effect, of T and pressure on $\epsilon_\perp$ measured at constant f. Application of pressure drastically alters riot only the mag-

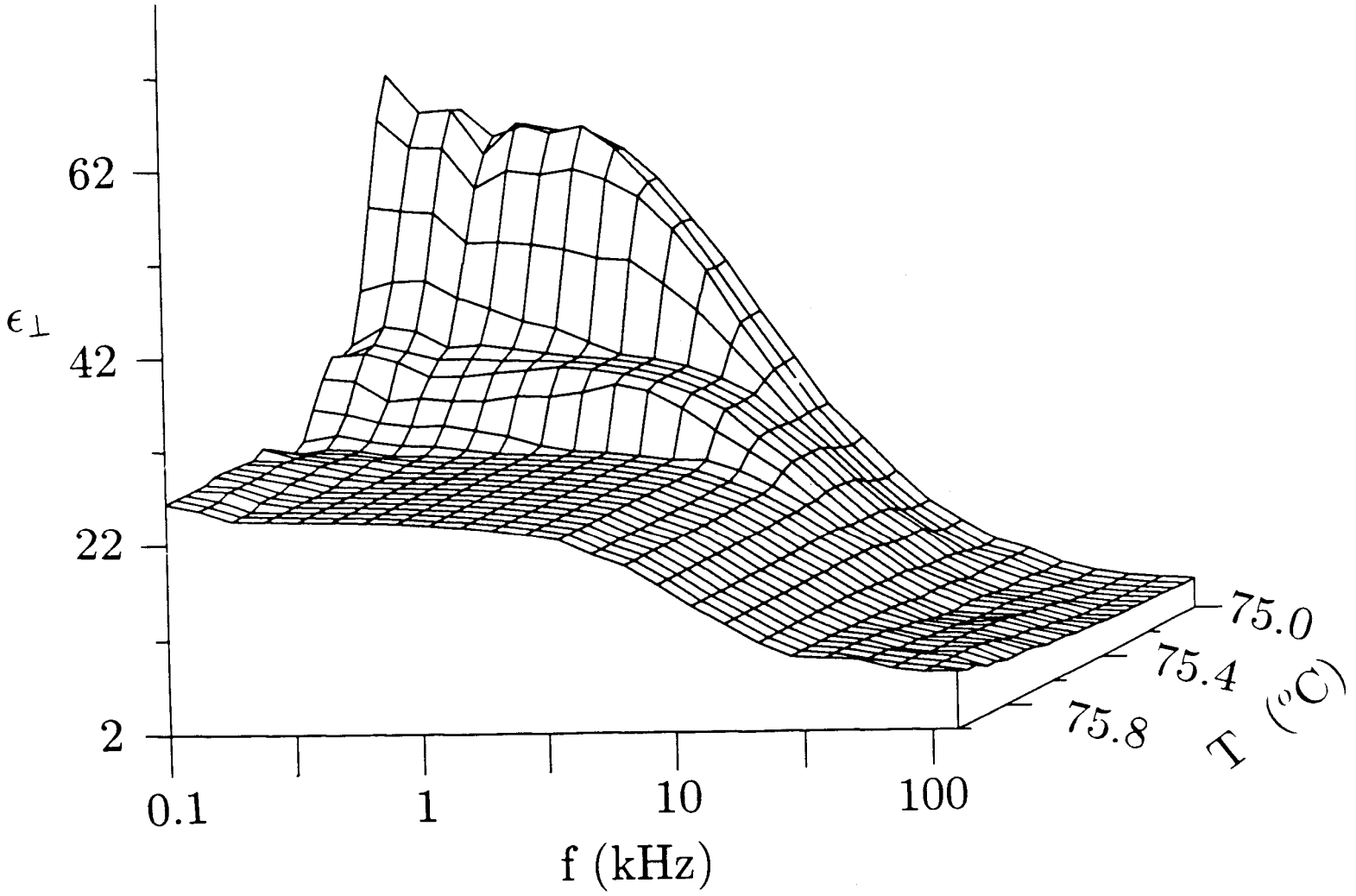

Fig.6.21(a). Surface plot showing soft mode relaxation in the A phase close to the transition.

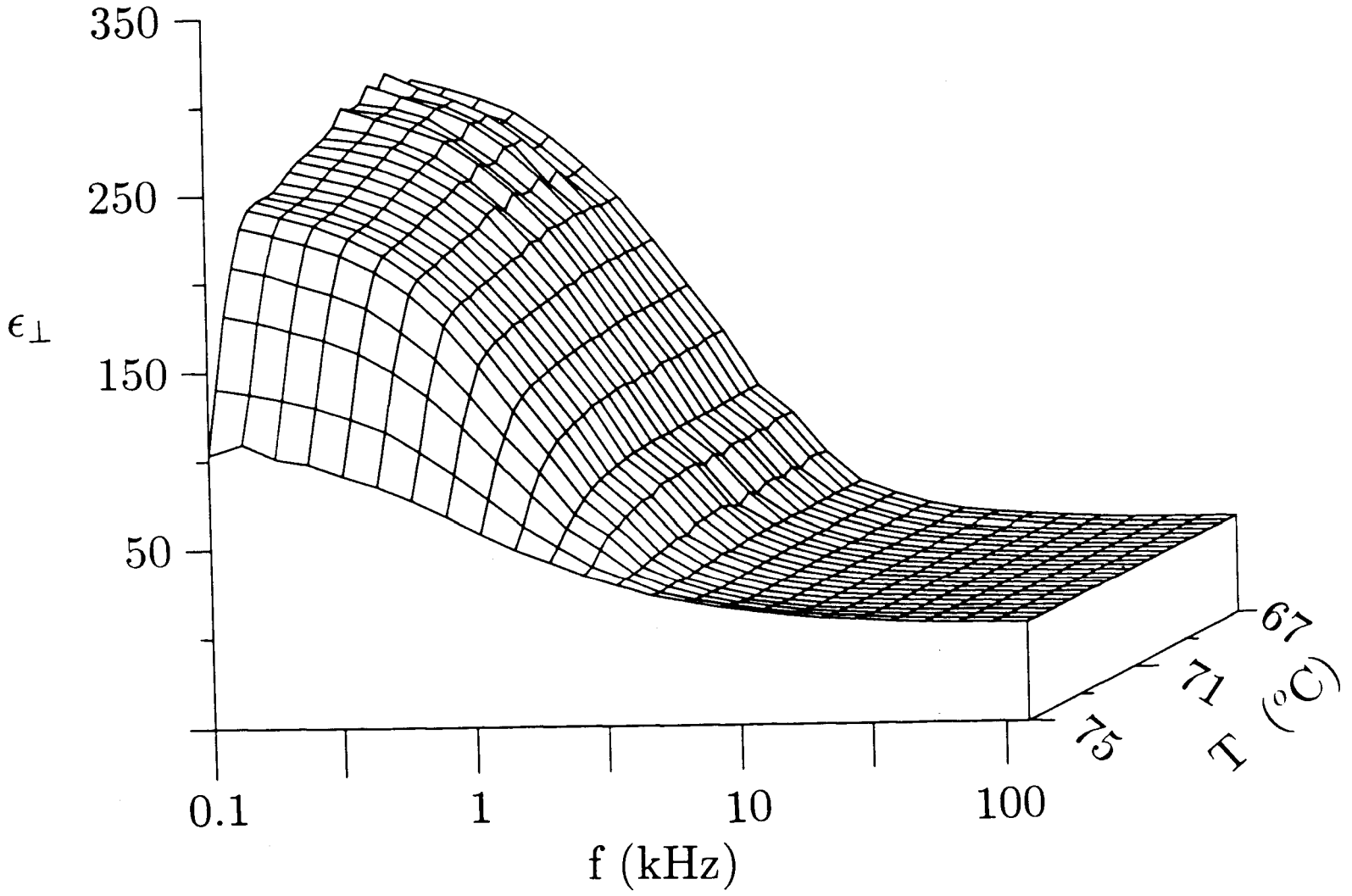

Fig.6.21(b). Surface plot showing Goldstone mode relaxation in the C^* phase close to the transition.

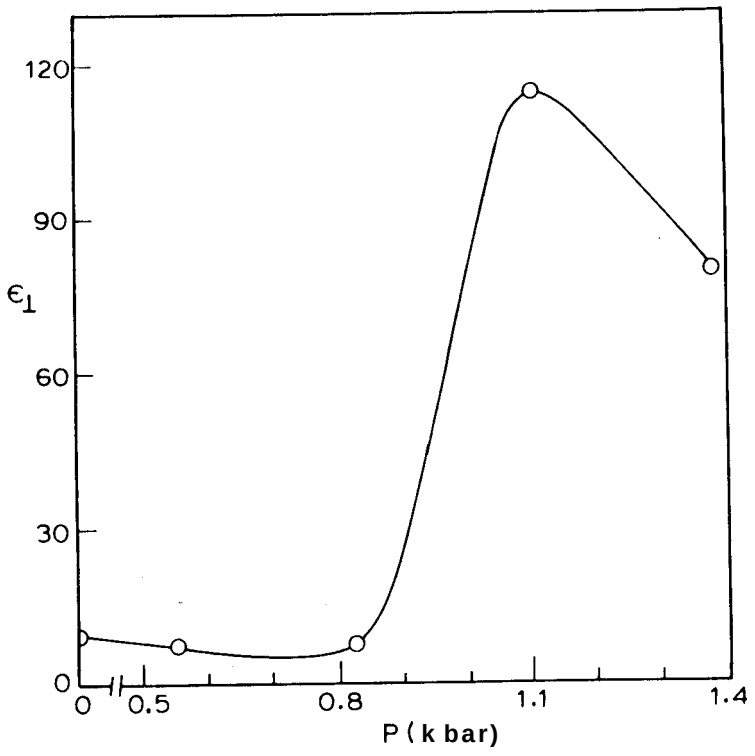

Fig.6.22(a). Variation of $\epsilon_\perp$ as a function of pressure at, T = 92°C and f = 50 Hz. The line is a guide to the eye.

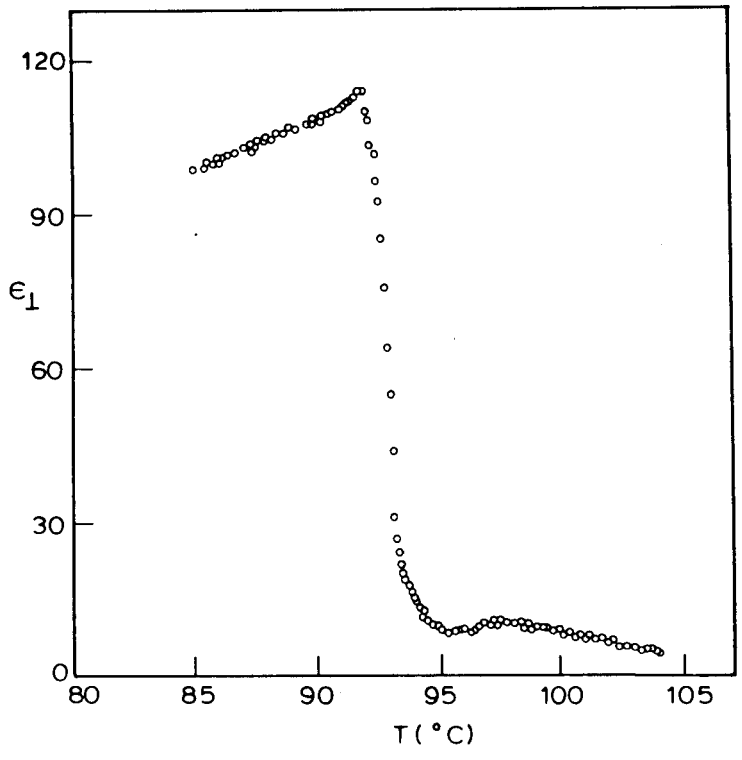

Fig.6.22(b). Thermal variation of $\epsilon_\perp$ at P = 1.1 kbar and f = 50 Hz.

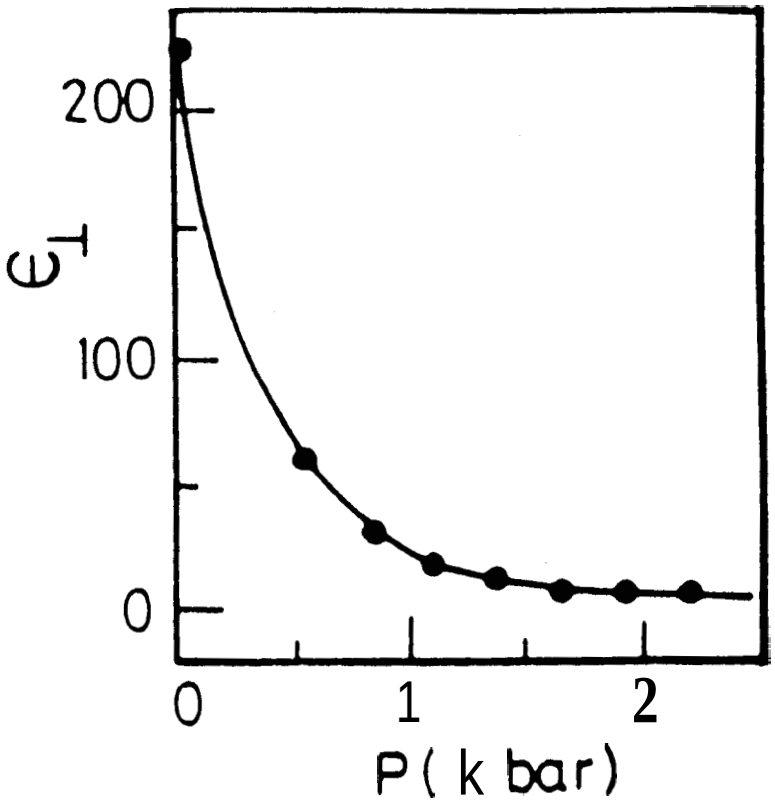

Fig.6.23. Pressure dependence of $\epsilon_\perp$ at $T_c - 4°C$.

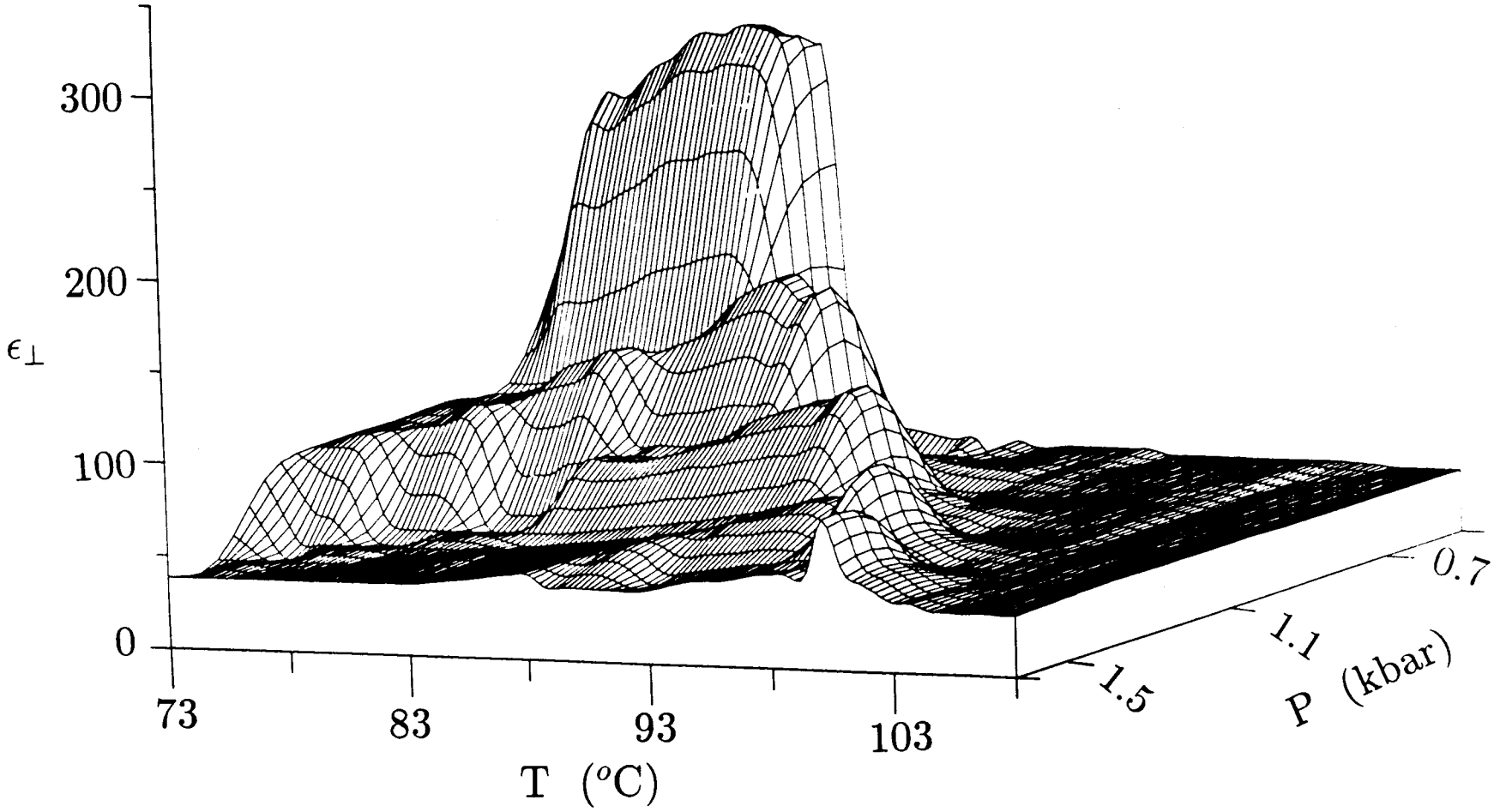

Fig.6.24. Perspective view of the effect of temperature and pressure on $\epsilon_\perp$

nitude of $\epsilon_\perp$ but also brings about significant changes in the shape of its thermal variations. This is true over a wide range of frequencies as seen from figures 6.25 to 6.29. When the frequency is low (50 Hz) the shape does riot change much but the value of $\epsilon_\perp$ decreases substantially with increasing pressure. When $j = 200$ Hz (Fig. 6.26) tlie data for $\Gamma = 0.5$ kbar resembles tlie $\epsilon_\perp$ behaviour at room pressure. The profile for $P = 0.83$ kbar is remarkably different. In the transition region there is a sharp peak followed by a secondary - hut less conspicuous - peak. On increasing the pressure further tlie shape of the profile remains more or less the same except for minor changes. The behaviour at higher frequencies (1, 10 and 40 KHz) are shown in Figures 6.27-6.29. Similar features have been seen at room pressure when an external field like magnetic or electric (DC bias) fieltl is applied normal to the helix. This effect is attributed to the unwinding of the helix and a consequent suppression of the Goldstone mode. Extending the argument to the present case. One can pressume that tlie behaviour seen at high pressure is due to the suppression of GM.

As noted earlier in chapter III, tlie strength of soft mode (SM) reaches a maximum at T_c. Thus the peaks seen in tlie profiles obtained at higher frequencies can he associated with the existence of the SM relaxation. Notice further that the peak heights decrease with increasing pressure and hence the strength of the soft mode may also be decreasing. In other words, "the relaxation parameters of both the director modes (GM & SM) appear to be influenced by the application of pressure". The evidence for this is shown in figures 6.30 and 6.31 where $\epsilon_\perp$ is plotted against frequency on a semilogarthmic scale for $P = 1$ bar and 1.1 kbar in the A and C* phases respectively. These figures show in a striking fashion that the relaxation frequencies of both the modes decrease substantially on increasing the pressure. Therefore, one

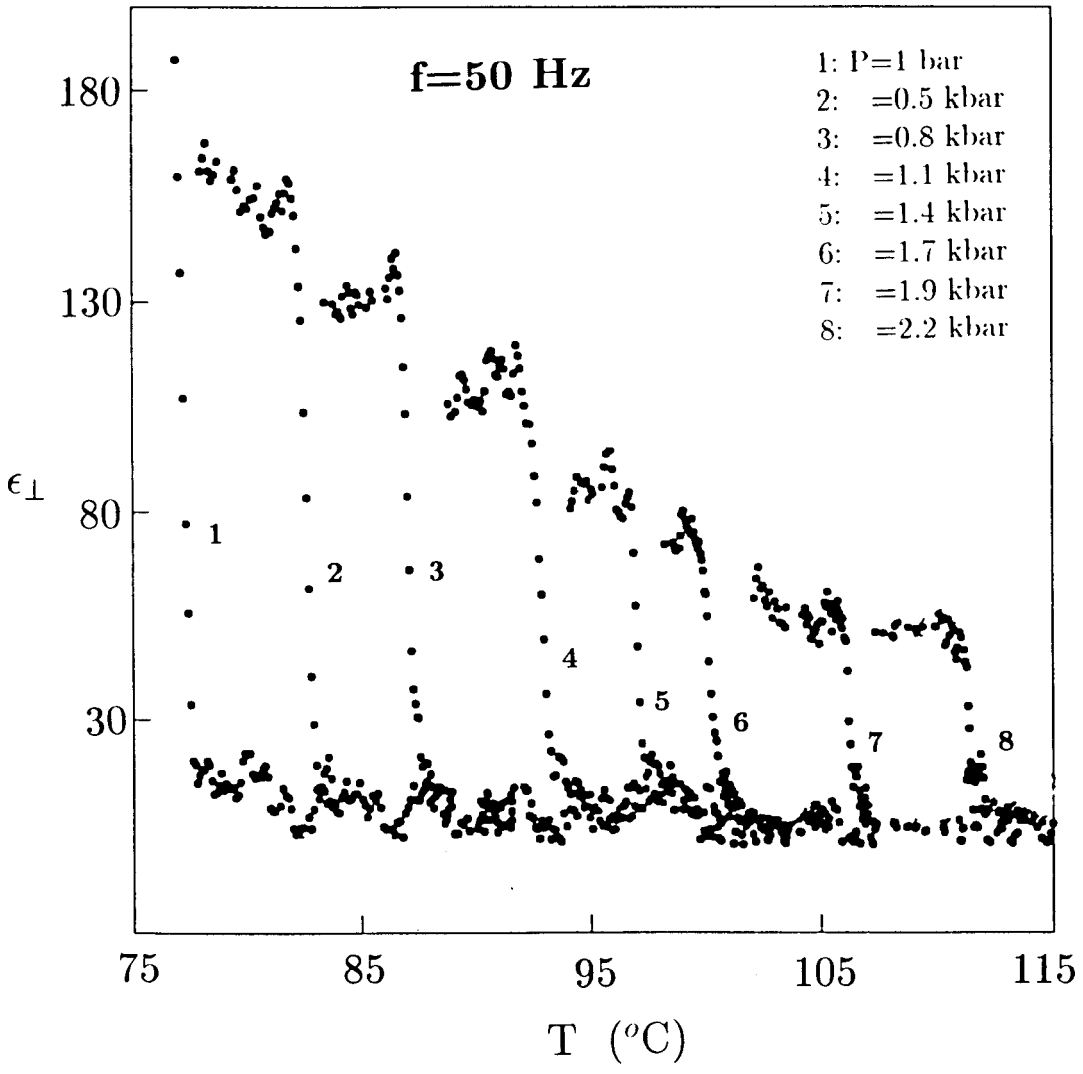

Fig.6.25. Thermal variation of $\epsilon_\perp$ for f = 50 Hz at different pressures.

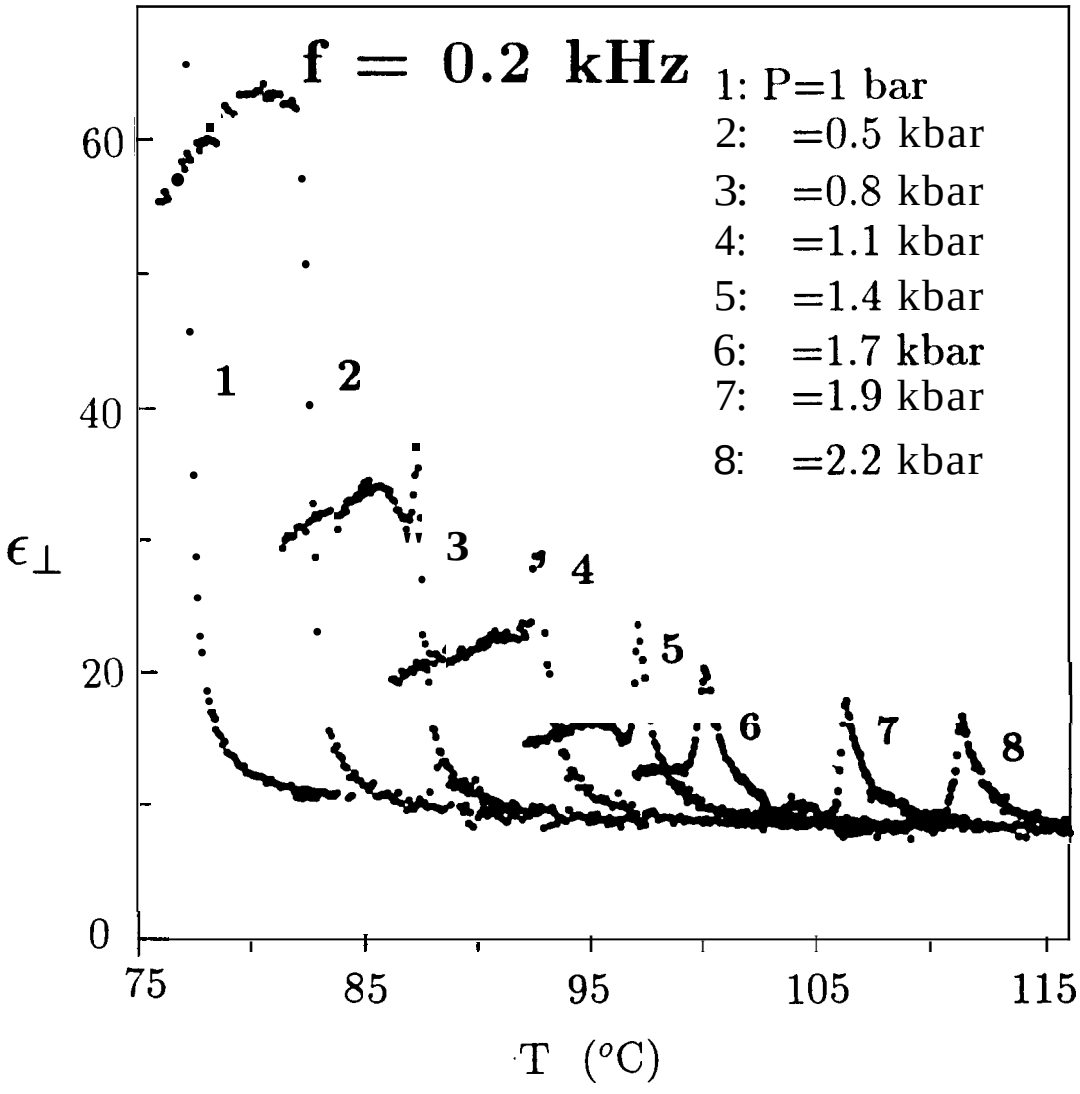

Fig.6.26. Temperature dependence of $\epsilon_\perp$ for f = 200 Hz at different pressures.

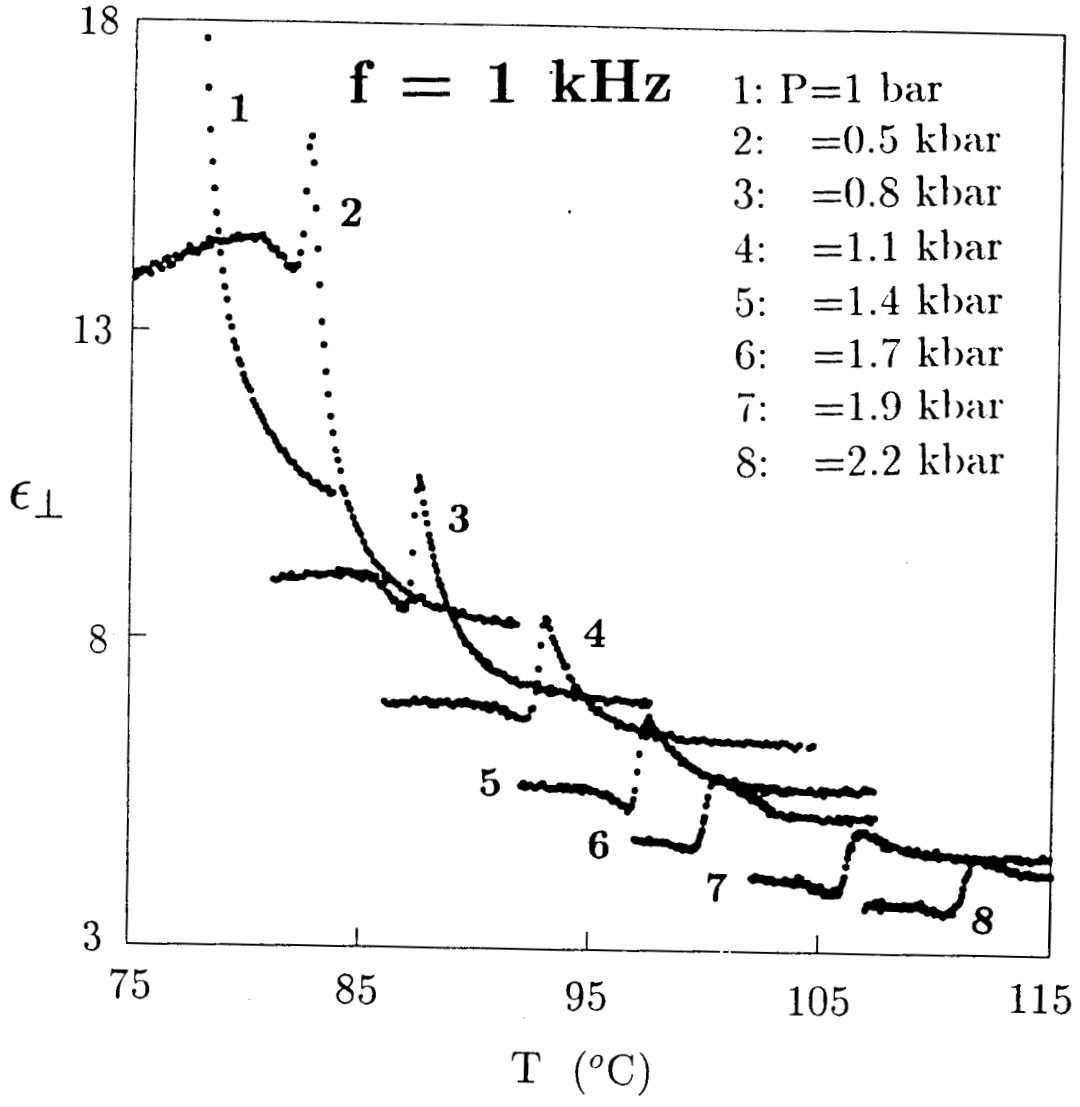

Fig.6.27. $\epsilon_\perp$ vs. temperature for $f = 1$ kHz. at different pressures.

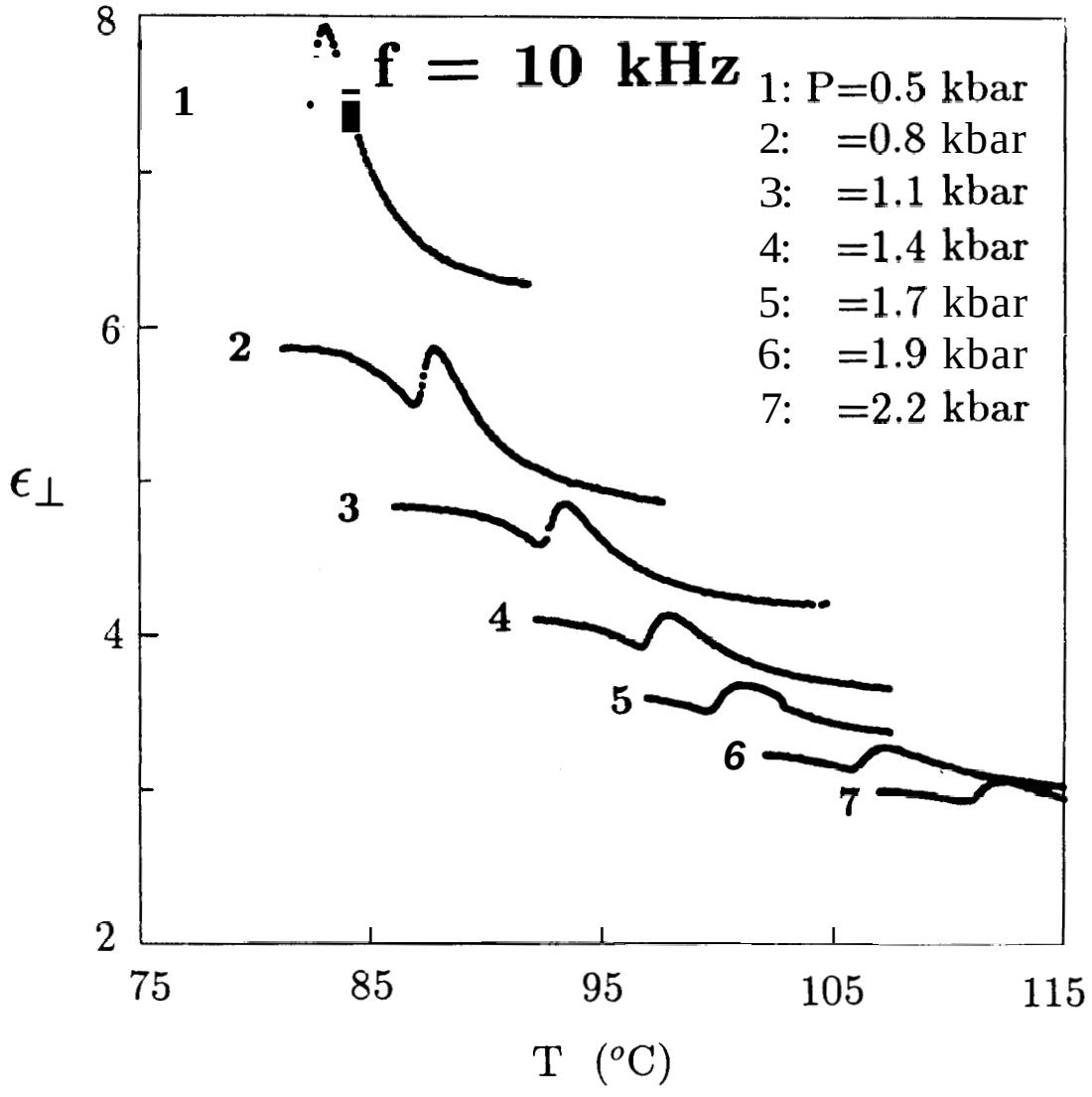

Fig.6.28. $\epsilon_\perp$ vs. temperature for $f = 10$ kHz. at different pressures.

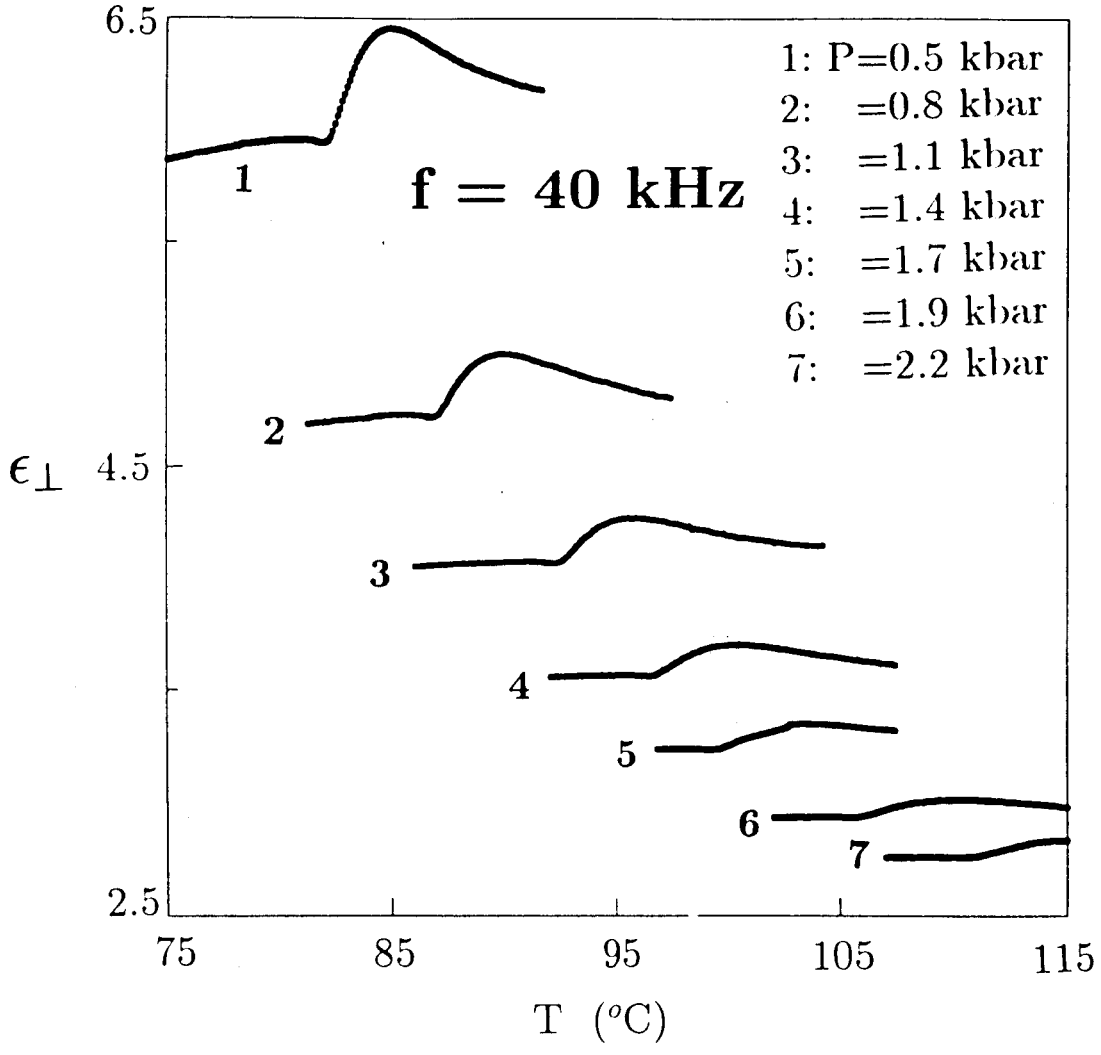

Fig.6.29. $\epsilon_\perp$ vs. temperature for $f = 40$ kHz. at different pressures.

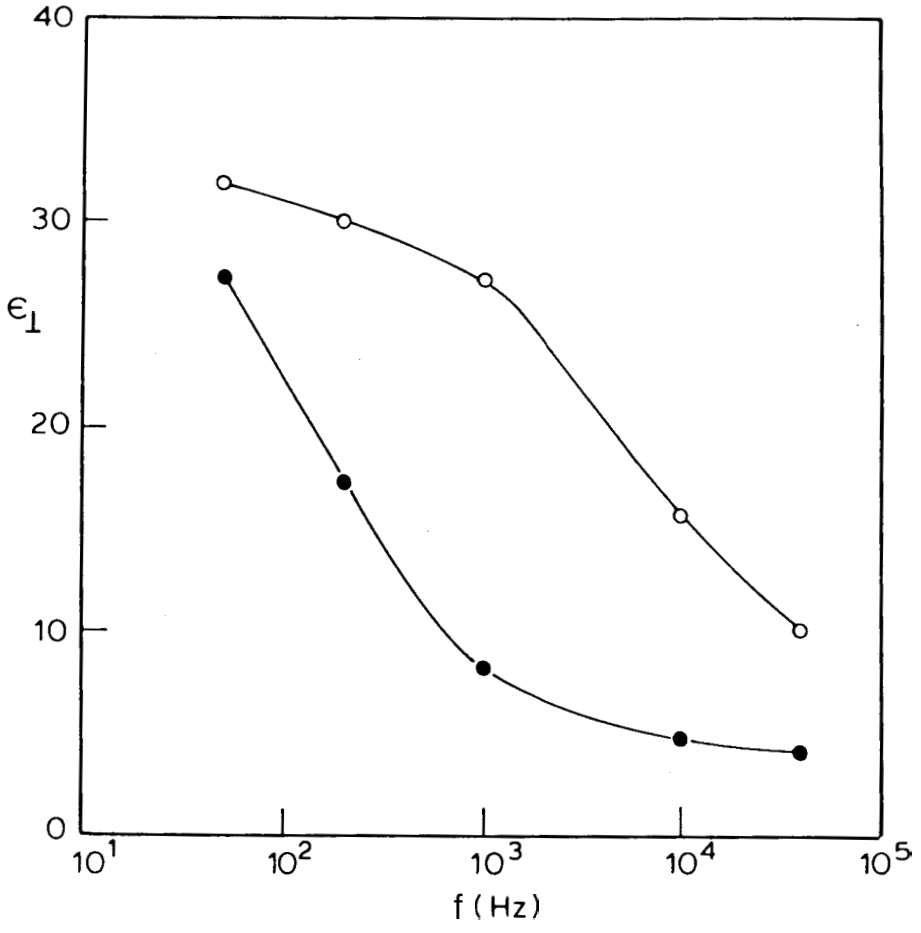

Fig.6.30. Semi-logarithmic plot, of $\epsilon_\perp$ vs. frequency in the A phase at $P = 1$ bar (○) and 1.1 kbar **(a)** The lines are meant to serve as guide to the eye.

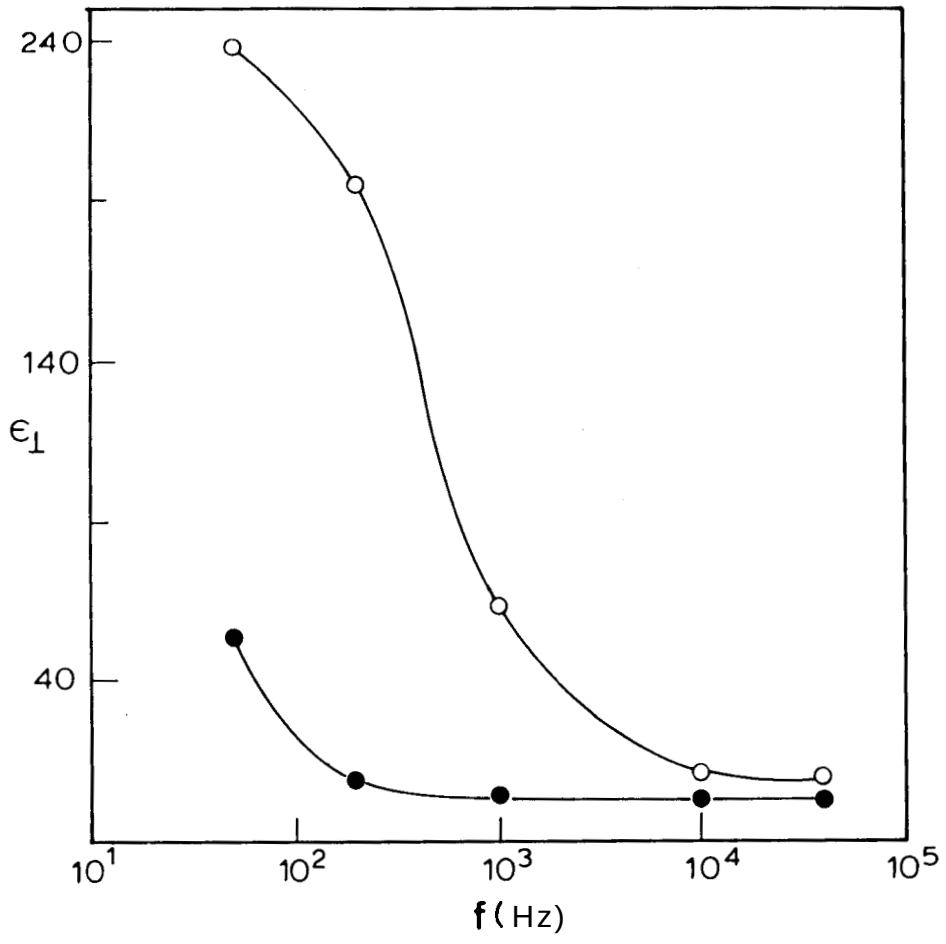

Fig.6.31. $\epsilon_\perp$ vs. frequency in the C^* phase at P = 1 bar (○) and 1.1 kbar (●). The lines are guide to the eye.

can conclude that tlie application of pressure slows clown the dynamics of the system. We have seen earlier in section 6.3.3 that the rotational viscosity γ_ϕ, associated with tlie Goldstone mode switching, increases with increasing pressure. It is also known that the GM frequency f_G can be written as[19,20]

$$f_G = \frac{K_3 q^2}{2\pi\gamma_\phi} \tag{6.1}$$

Thus the substantial increase seen for γ_ϕ could be one of the prime reasons for the decrease in f_G.

To extract the information regarding the SM relaxation, we make use of the $\epsilon_\perp$ data collected in the *A* phase where GM does not exist. For this purpose we have treated the raw $\epsilon_\perp$ data obtained at 200 Hz, after subtracting ϵ_∞, to be equal to $\Delta\epsilon_s$, the strength of SM. This is a valid procedure since the dispersion data obtained at 1 bar show that f_s, which would be minimum at the transition, is much higher than 200 Hz. Here ϵ_∞ represents tlie sum of the dielectric strengths of all other high frequency modes. (We make the assumption that well above the transition, T_c + 7°C, $\epsilon_\infty = \epsilon_\perp$.) According to the generalized Landau model, the strength of SM is given by[2'] (ignoring the $\epsilon\mu^2$ term)

$$\frac{1}{\Delta\epsilon_s} = A(T - T_c) + B \tag{6.2}$$

where

$$A = \frac{a}{\epsilon^2 C^2} \tag{6.3}$$

and

$$B = \frac{K_3 q_o^2}{\epsilon^2 C^2} \tag{6.4}$$

a being tlie coefficient of the first term in the Landau expansion, ϵ the high temperature dielectric susceptibility, C is tlie bilinear coupling coefficient, K_3 an elastic

constant and q_o is the wavevector of the helix at the transition. From eqn. 6.2 it is clear that the value of $(1/\Delta\epsilon_s)$ decreases as $T \rightarrow T_c$ and reaches a minimum value (=B) at. T_c. Thus B of eqn. 6.4 is the inverse of $\Delta\epsilon_s$ at T_c. In figure **6.32** we have plotted B as a function of pressure. And it is seen that B varies linearly with pressure with a slope of 1.7 x 10^{-3}/kbar.

Since ***a*** and C are not known, we write eqn. 6.2 as,

$$\tilde{\Delta}\epsilon = \frac{\Delta\epsilon_{peak}}{\Delta\epsilon_s} = \frac{A}{B}(T - T_c) + 1 \qquad (6.5)$$

where $\Delta\epsilon_{peak}(= \frac{1}{B})$ is tlie value of At, at T_c. Thus a plot of this "reduced dielectric strength" against T – T_c should be a straight line having a slope of $\frac{A}{B}(= \frac{a}{K_3 q_o^2})$. Figure 6.33 is a plot of $\tilde{\Delta}\epsilon$ vs. $T - T_c$ for several pressures. $\tilde{\Delta}\epsilon$ is found to be linear close to T_c and departs from it on moving away from T_c. It may be mentioned here that the sortie observations of non-linear thermal variation of $\frac{1}{\Delta\epsilon_s}$ have been made earlier.[22–24] Fitting the data close to T_c (up to $T_c + 0.5)^o$C to a straight line by fixing the intercept to be equal to one, we have calculated the value of A/B at different pressures. The variation of A/B as a function of pressure is shown in figure 6.34. It is seen that A/B varies non-linearly with pressure.

Thus our measurements throw some light on the pressure variation of P,, γ_ϕ, E_c and $\epsilon_\perp$. However, measurements of θ, K_3 and q as a function of pressure would provide a better understanding of the effect of pressure on ferroelectric properties of FLCs.

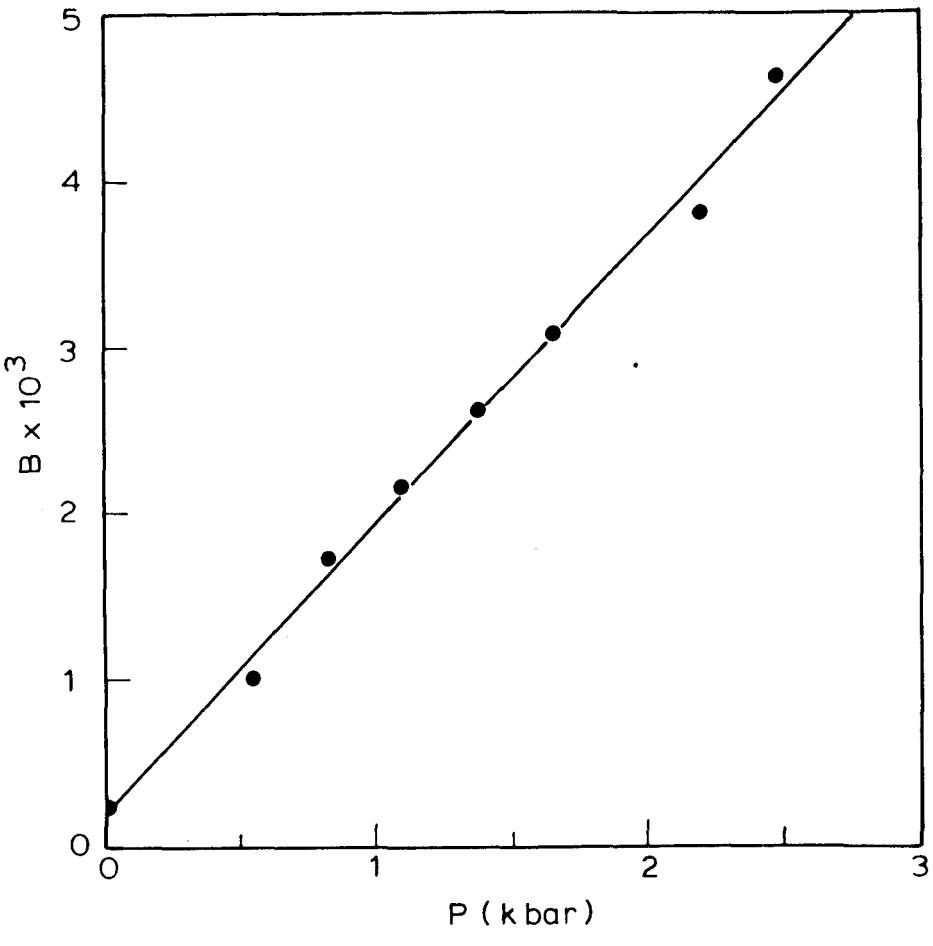

Fig.6.32. Pressure dependence of the quantity B (inverse soft mode strength at the transition). The line is a straight line fit to the data, with a slope of 1.7 x 10^{-3}/kbar.

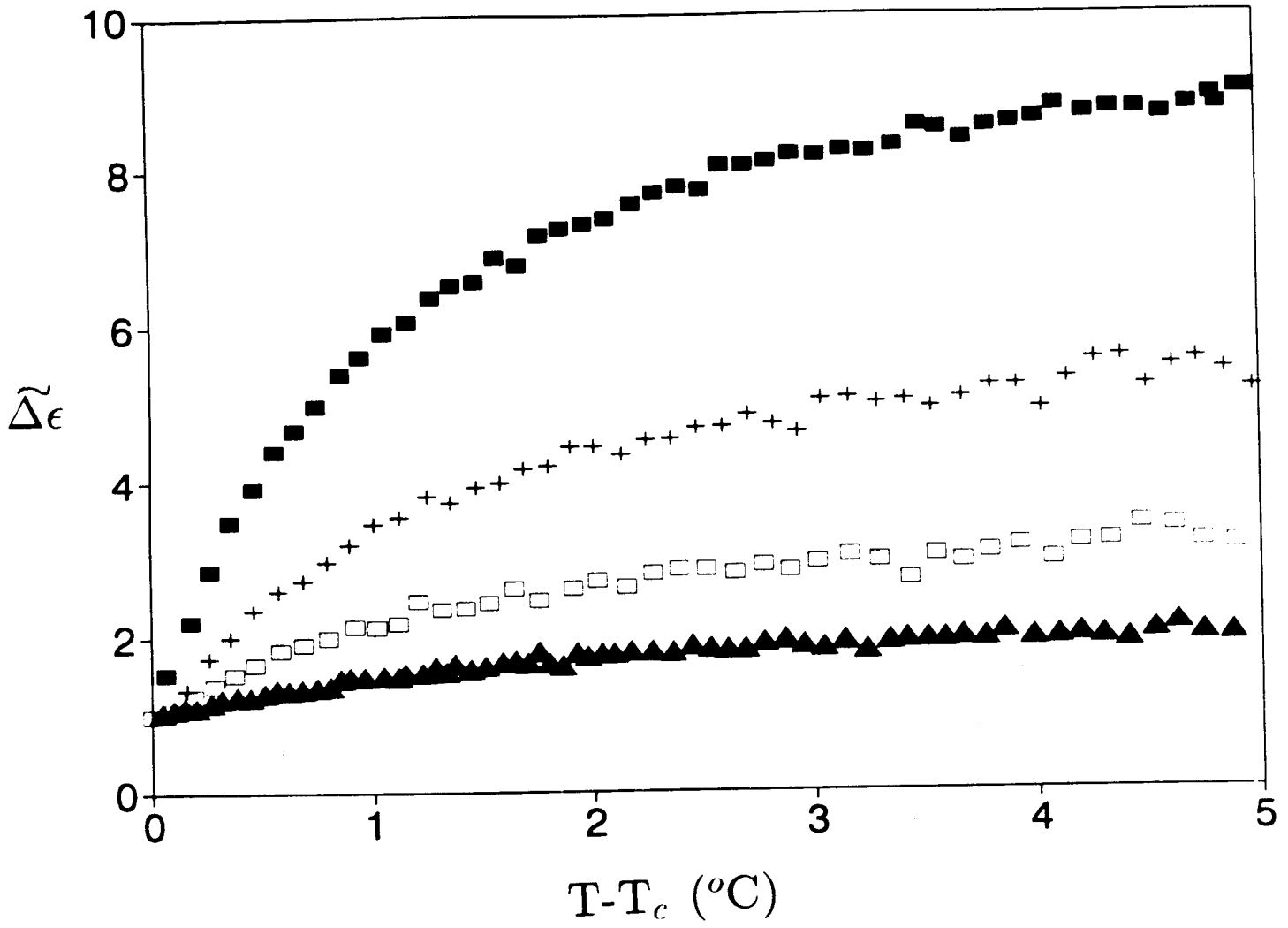

Fig.6.33. Plot of reduced $\Delta\epsilon_s$ vs. $T - T_c$ at 1 bar (■), 0.5 kbar (+), 1.1 kbar (□) and 2.2 kbar (▲).

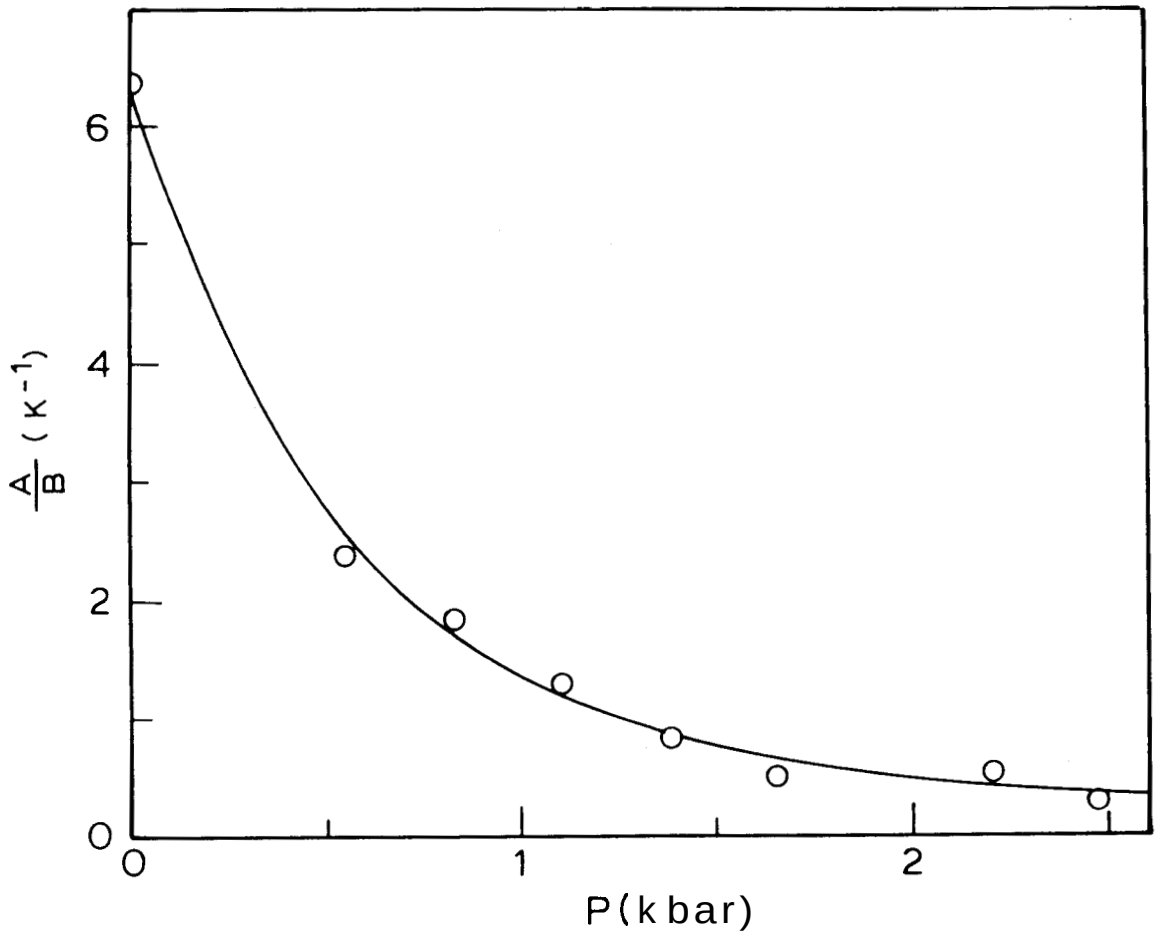

Fig.6.34. Plot of the ratio A/B vs. pressure. The line is guide to the eye.

References

[1] S.Chandrasekhar and R.Shashidhar, Advances in Liquid Crystals, Vol. 4, Ed. G.H.Brown (Academic Press, 1979), p. 83.

[2] R.Shashidhar, B.R.Ratna and S.Krishna Prasad, *Phys. Rev.* Lett., 53, 2141 (1984).

[3] D.Guillon, J.Stamatoff and P.E.Cladis, J. *Chem.* Phys., 76, 2056 (1982).

[4] S.Krishna Prasad, B.R.Ratna, R.Shashidhar and V.Surendranath, *Ferroelectrics*, 58, 101 (1984).

[5] N. Yasuda, S.Fujimoto and S.Funado, J. Phys. *D* : Appl. *Phys.*, **18,** 221 (1985).

[6] M.Ozaki, N. Yasuda and K.Yoshino, *Jpn.* J. Appl. Phys., 26, L1927 (1987).

[7] M. Ozaki, K.Nakao, T.Hatai and K.Yoshino, Liquid Crystals, 5, 1219 (1989).

[8] A detailed description of the original set-up and its modifications are given in A.N.Kalkura, R.Shashidhar and M.S.R. Urs, J. Physique, 44, 51 (1983); R.Shashidhar, S.Krishna Prasad and S.Chandrasekhar, *Mol. Cryst.* Liquid *Cryst.*, **103,** 137 (1983).

[9] S.Krishna Prasad, *High Pressure Studies* of *Liquid* Crystalline *Transitions*, Ph. D. Thesis, University of Mysore (1985).

[10] B.Shivkumar, B.K.Sadashiva, S.Krishna Prasad and S.M.Khened, *Ferroelectrics*, **114,** 273 (1991).

[11] J.S.Patel, T.M.Leslie and J.W.Goodby, *Ferroelectrics*, 59, 137 (1984).

[12] H.Diamant, K.Drenck and R.Pepinsky, *Rev.* Sci. *Instrum.*, 28, 30 (1957).

[13] C.Escher, H.R.Dubal, W.Hemmerling, I. Muller, D.Ohlendorf and It.Wingen, *Ferroelectrics*, 84, 89 (1988).

[14] C.C.Huang and S.C.Lien, Phys. *Rev.*, A31, 3621 (1985).

[15] S.Krishna Prasad, V.N.Raja, D.S.Shankar Rao, Geetha' G. Nair and M.E.Neubert, *Phys.* Rev., A42, 2479 (1990).

[16] C.C.Huang, *Mol. Cryst.* Liquid *Cryst.*, 144, 1 (1987).

[17] R.Shashidhar, B.R.Ratna, Geetha G. Nair, S.Krishna Prasad, Ch. Bahr and G.Heppke, Phys. Rev. Lett., 61, 547 (1988).

[18] H.Y.Liu, C.C.Huang, T.Min, M.D.Wand, D.M.Walba, N.A.Clark, Ch. Bahr and G.Heppke, Phys. Rev., A40, 6759 (1989).

[19] A.Levstik, T.Carlsson, C.Filipic, I.Levstik, arid B.Zeks, *Phys.* Rev., A35, 3527 (1957).

[20] Ph. Martinot-Lagarde and G.Durand, J. Physique, 41, L-43 (1980).

[21] T.Carlsson, B.Zeks, C.Filipic and A.Levstik, Phys. *Rev.*, A42, 877 (1990).

[22] J.Pavel and M.Glogarova, *Ferroelect*rics, 84, 241 (1988).

[23] F.Gouda, K.Skarp and S.T.Lagerwall, *Ferroelectrics*, 113, 165 (1991).

[24] S.U.Vallerien, F.Kremer, H.Kapitza, R.Zenter and W.Frank, *Phys.* Lett., **A138**, 219 (1988).